Polymer Composites

WILEY | spe INSPIRING PLASTICS PROFESSIONALS

RESEARCH ARTICLE

Effect of Carbon Nanotube Reinforcement on Glass Fiber Thermoplastic Laminates: Elastic Properties, Impact Resistance, and Electrical Conductivity

A. Y. E. Kouassi[1] | R. Matadi Boumbimba[2] | M. K. Sangaré[2] | T. Libura[3] | I. Royaud[4] | P. Dziewit[5] | M. Wary[2]

[1]Institut National Polytechnique Félix HOUPHOUËT-BOIGNY de Yamoussoukro, UMRI STI-Laboratoire de Mécanique, d'Energétique et de Sciences des Matériaux (LAMESMA), Yamoussoukro, BP, Côte d'Ivoire | [2]CNRS, Arts et Métiers ParisTech, LEM3, Université de Lorraine, Metz, France | [3]Institute of Fundamental Technological Research of the Polish Academy of Sciences, Warsaw, Poland | [4]Université de Lorraine, CNRS, Institut Jean Lamour (IJL), Nancy, France | [5]Military University of Technology, Faculty of Mechatronics and Aviation, Warsaw, Poland

Correspondence: R. Matadi Boumbimba (rodrigue.matadi-boumbimba@univ-lorraine.fr)

Received: 30 March 2026 | **Revised:** 7 June 2026 | **Accepted:** 9 June 2026

Keywords: elastic properties | electrical conductivity | Graphistrength MWCNT | impact resistance | laminate composite

ABSTRACT

Glass fiber/Elium acrylic thermoplastic laminate containing various weight fractions of multiwalled carbon nanotubes (Graphistrength MWCNTs) was subjected to tensile, low-velocity impact, and dielectric tests, and compared to a control composite without MWCNTs. The composite materials were manufactured via vacuum resin infusion following manual preimpregnation of the reinforcement phase. The results showed that integrating from 1 to 2.5 weight fraction (wt%) of MWCNTs enhanced both elastic properties and impact resistance. Specifically, the Young's modulus increased by more than 18% relative to the pristine composite. Under impact energies of 40 and 60 J, the MWCNT-reinforced composite exhibited a 15% increase in peak force, a 16.4% reduction in absorbed energy, and a 30% enhancement in the penetration threshold. Improvement in mechanical performance could mainly be due to the good MWCNT–fibers–matrix adhesion which creates strong bonding between glass fibers and MWCNT, thereby improving stress transfer. Concurrently, the composite materials became electrically conductive starting at 2 wt% of MWCNTs, suggesting a high probability of interconnected MWCNT particles and indicating the percolation threshold. While 2 wt% can be considered as the optimal MWCNT content for overall properties, an exceptional 680% increase in electrical conductivity was achieved at 3.5 wt%.

1 | Introduction

In recent decades, improving the properties of thermoplastic laminate composites has been a major interest for industries involved in the advancement of composite materials. For this purpose, ARKEMA company developed an acrylic liquid resin named Elium, which offers strong adhesion with various fibers such as glass, aramid and carbon. Elium acrylic resin enables the production of glass fibers composites with high mechanical performance, while also providing the advantages of postformability and recyclability. Indeed, glass fibers laminates based on Elium acrylic matrices have demonstrated not only excellent mechanical properties [1, 2], but also improved low velocity impact resistance [3–5] compared to composites with thermoset matrices. However, the major limitation of polymer laminate composites is their reduced resistant to early damage mechanisms such as matrix cracking, delamination and fiber breakage [6–8]. To overcome these weaknesses, several strategies have been explored, including the incorporation of nanometric reinforcements alongside conventional microscopic fibers. For example, block copolymers can enhance impact resistance through strong adhesion between copolymer and polymer matrix chains, as well as micelles cavitation within the composite [9–11]. Since polymer

Highlights

- Hand lay-up process allows for good nanoparticle-fibers–matrix adhesion.
- Elastic properties increase with up to 2.5 wt% of carbon nanotube content.
- Absorbed energy trends closely follow those of the elastic properties.
- Penetration threshold is optimized at 1 wt% of carbon nanotube content.
- Percolation threshold is reached at 2 wt% of carbon nanotube content.

matrices, glass fibers, and blocs copolymers are dielectrics [12], the resulting laminates provide only good impact properties. Consequently, these composite materials are limited in applications requiring electrical conductivity. To address this limitation, carbon nanotubes, particularly, multiwalled carbon nanotubes (MWCNT) have been introduced as nanoscale reinforcements in fiber-reinforced polymer composites [13–16]. MWCNT not only improve mechanical properties but also significantly increase electrical conductivity. These enhancements are attributed to their exceptionally high Young's modulus (~ 1 TPa) and large aspect ratio ($100 - 1000$) which enable efficient stress transfer and electrical percolation [17–21]. Moreover, MWCNT form multiple bonds within the polymer matrix due to their multiwall structure, in contrast to single-walled carbon nanotubes, as reported by Fulmali et al. [22]. Functional groups on MWCNT walls further promote strong chemical bonding and interfacial adhesion through Van der Waals-type interactions [23]. For glass fiber/polymer matrix composites containing MWCNT, mechanical properties may depend on fiber volume fraction and testing temperature, as noted by Md Nadeem et al. [15]. In studies on short glass fibers/epoxy composites reinforced with MWCNT, an increase in ultimate tensile strength of about 20.7% was achieved with 1.5 wt% MWCNT at 25°C and a fiber volume fraction of 8.5%. However, tensile tests conducted at 180°C showed a 79.68% decrease in ultimate tensile strength for the same composite, likely due to fiber–matrix decohesion caused by elevated temperature. For long fiber laminate composites, property improvements with the addition of MWCNT are even more pronounced, as demonstrated by Dheepthi et al. [24]. By adding 1 wt% MWCNT to glass fiber/epoxy laminates, tensile strength and the Young's modulus increased on average by 34.51% and 44.15%, respectively, compared to the neat composite. These improvements also extended to compressive, flexural, and interfacial shear strength. According to these authors, the significant improvement in mechanical properties was due to MWCNT impregnation of the glass fabric, which enhanced adhesion between glass fibers, carbon nanotubes, and the epoxy matrix. Dalina et al. [25] demonstrated that adding 2.8 wt% MWCNT to glass fibers/epoxy composite increased flexural strength and modulus by 50% and 13%, respectively, compared to composites without MWCNT. This improvement was attributed to strong fiber-MWCNT adhesion. However, the hybrid composites studied exhibited porosities, resulting in lower densities compared to composites without MWCNT. Porosities can be advantageous in composites when lightweight structures are required. However, porosities is generally unfavorable, as it reduces fiber–matrix bonding and decreases stiffness and strength [26]. In the study by Yoganandam et al. [27], a steady increase in tensile and flexural strength of glass fiber/epoxy composites was observed with MWCNT contents ranging from 0.5 to 2 wt%. At 2 wt% of MWCNT, tensile and flexural strength increased by 35% and 23%, respectively, compared to the neat composite. For the same MWCNT content, interlaminar strength increased by 205%. These enhancements were attributed to strong fiber-matrix interfacial adhesion provided by MWCNT. In most hybrid composites, property improvements appear to stem from the strong bonding ability of MWCNT to both fibers and matrix. According to Gaurav and Singh [28] and Domun et al. [29], MWCNT adhesion to fibers increases the load-bearing area due to their high aspect ratio, enabling more effective stress transfer to the fibers. Furthermore, the high tortuosity of MWCNT creates barrier-like pathway in the microstructure, making interfacial delamination more difficult. As a result, this adhesion hinders composite damage mechanisms such as matrix crack initiation and propagation, delamination, and fiber breakage. Moreover, carbon nanotubes can absorb deformation energy under different loading conditions [30, 31]. Depending on the loading type, ply stacking sequences can influence the overall properties of MWCNT-based hybrid composites, as reported by Radhakrishnan and Ramajeyathilagam [32] in their study on glass fiber ($\pm 45°$)/epoxy composites. With 1 wt% of MWCNT, their results showed increase in tensile strength and Young's modulus of 23.30% and 18.75%, respectively, compared to the unreinforced composite. However, MWCNT appeared to have no positive effect on compression behavior. Indeed, fibers tend to slip within the matrix until they align with the loading direction, in which case composite strength mainly depends on fiber-matrix interfacial adhesion, as stated by Singh et al. [33]. The presence of MWCNT enhances matrix extension, explaining the high deformation and resulting property improvements [30]. For compression, the authors noted that property reduction were due to nonuniform distribution of MWCNT particles in the microstructure. Regarding ply stacking sequences, MWCNT orientation can also influence the properties of hybrid composite, as reported in [22]. The authors demonstrated that aligning MWCNT through the ply thickness using a 600 V alternating current significantly improved flexural properties, as the carbon nanotubes formed barriers to crack propagation oriented along the fiber direction [34]. To further enhance fiber-matrix adhesion, carbon nanotubes are often modified with specific dispersing agents during processing. For instance, Ismail et al. [35] observed increases in flexural strength and modulus of 54% and 24%, respectively, by using MWCNT modified with Gum Arabic (GA) to reinforce glass fiber/epoxy composites. This performance was achieved with 0.1 wt% MWCNT/GA, due to good carbon nanotubes dispersion attributed to steric stabilization by nonionic surfactants such as GA, which possess a hydrophilic head and a hydrophobic tail. The hydrophobic tail adsorbs onto the MWCNT surface, while the hydrophilic segments extend into the aqueous solution, creating a potential barrier between carbon nanotubes. Good dispersion also promoted better fiber–matrix interfacial adhesion, leading to an increase in

interlaminar strength of about 26.7% compared to the unreinforced laminate. Jelmy et al. [36] modified MWCNT using aniline ammonium persulfate $(NH_4)_2S_2O_8$ (APS), producing MWCNT/PANi. The Young's modulus of glass fiber/epoxy composites with 2.5 wt% MWCNT/PANi increased to a maximum value of about 6 GPa, beyond which a decline was observed. The increase in Young's modulus was 400% higher than that of the composite without MWCNT and was attributed to PANi modification. PANi coatings, well anchored to MWCNT, reacted with polymer chains during polymerization, resulting in strong interfacial adhesion between the matrix and PANi. This performance was attributed to the stronger covalent bonds provided by MWCNTs/PANi, which limited polymer chain mobility [37]. This adhesion enabled more effective stress transfer from the MWCNTs/PANi-modified matrix to the fibers, reinforcing the composite, as reported by Xu et al. [38]. The drop in Young's modulus was attributed to the high viscosity of the epoxy/MWCNTs/PANi mixture, which reduced dispersion quality beyond 2.5 wt% MWCNT/PANi.

Adding MWCNT to polymer laminate composites can also improve electrical conductivity in several applications [10, 17]. As reported in [38], electrical conductivity increased up to 0.5 wt% MWCNT and reached a maximum at 3 wt%, due to strong adhesion of MWCNTs/PANi on glass fibers, which improved interconnections between carbon nanotubes. A similar trend was observed by He et al. [39] in glass fiber fabrics/epoxy composites, where electrical conductivity significantly increased up to 2 wt% of CNT content. According to the authors, the increase in conductivity was attributed to CVD-grown CNTs/GFFs processing, which promoted good CNT structure and alignment on glass fabrics. MWCNT can also improve the mechanical and dielectric properties of hybrid glass- natural fiber laminates. Mohan et Rajmohan [40] studied glass-flax fibers/epoxy composites and found that adding 1 wt% MWCNT improved tensile strength and flexural load by about 28.26% and 16.84%, respectively, compared to composite reinforced with neat glass-flax fibers. Using the dip-dry coating method to prepare MWCNT-reinforced composites can enhance properties, as reported by Kim et al. [41] in their study on MWCNT-coated basalt fibers/epoxy composites. Electrical conductivity significantly increased with dip-dry coating cycle, reaching a peak at 10 cycles, with composites containing about 2.65 wt% of MWCNT. According to the authors, this enhancement was due to well-formed interconnection networks of MWCNT coated on basalt fibers, which allowed electric charges to flow effectively along the interconnected nanotubes. Mendoue et al. [42] studied the thermomechanical behavior of flax/Elium acrylic composites reinforced with Graphistrength (MWCNT) (a multiwall carbon nanotube masterbatch developed by ARKEMA). Their results showed that composites with 2 wt% of MWCNT exhibited increases in Young's modulus and stress at break of about 27% and 23%, respectively, compared to composites with neat flax fiber. Electrical conductivity increased between 1 and 2 wt% MWCNT, reaching a peak at 2 wt%, about 68 times higher than that of neat flax fiber composites. Since flax fiber is dielectric and has a low Young's modulus, property improvement was attributed to the high tensile strength of MWCNT and their good adhesion to flax fibers, ensuring proper bonding with the Elium matrix. As explained above, using MWCNT as reinforcement in laminated composites is particularly important for improving mechanical and electrical conductivity. In the literature, numerous studies have focused on epoxy-based laminates. However, few studies have investigated Elium acrylic laminates modified with MWCNT, particularly glass fiber/Elium acrylic composites reinforced with MWCNT. Thus, the mechanical and electrical conductivity behavior of such composites remains largely unknown, offering an opportunity to study new recyclable materials.

This study focuses on enhancing the mechanical properties, impact resistance, and electrical conductivity of glass fibers/Elium acrylic laminates modified with various MWCNTs. Laminates were manufactured at room temperature using a hand lay-up process combined with vacuum resin infusion. As reported in the literature, achieving uniform integration of MWCNT into laminates remains a significant challenge for property enhancement. Therefore, this work evaluates the effect of incorporating Graphistrength via manual preimpregnation on the overall performance of glass fiber/Elium acrylic laminates. The synthesized composites were characterized using tensile, low-velocity impact, dielectric testing, and their performance was systematically compared to neat laminates. The primary objective of this work lies in identifying an optimal carbon nanotubes concentration that simultaneously guarantees superior mechanical properties (both elastic and low-velocity impact resistance) and excellent electrical conductivity.

2 | Materials and Processing

2.1 | Materials

The Elium acrylic resin used in this study is a thermoplastic liquid resin developed by Arkema's research group (lacq, France). Composed of an acrylic-based polymer, a reactive monomer, metal salts and additives, this formulation imparts a highly fluid behavior to the resin, which exhibits a translucent appearance and cures at room temperature ($\sim 20^{\circ}C$). The commercial and technical code assigned by Arkema for this specific formulation is E151 OSA resin. The acrylic resin has a kinematic viscosity of 110 cPs and a density of $1.18\,g/cm^3$, respectively. Furthermore, the E151 OSA resin possesses a Young's modulus of 3.3 GPa and a Poisson's ration of 0.4. The bidirectional glass fabric used was sourced from Chomarat company (le Cheylard, France). This woven glass fabric features a surface density of 800 g / m2 and the material density of $2.56\,g/cm^3$, respectively. The pattern frequencies in the warp and weft directions are 10 and 13.5 mm, respectively. The glass fabric has a Young modulus of 73 GPa and a Poisson ratio of 0.22. Both the E51 OSA resin and the woven glass fabric were provided by the Institute for Technological Research in Materials, Metallurgy, and Processes (IRT M2P, Composite Park Porcelette, France). Graphistrength CW2-L A1, also manufactured by Arkema's research group (lacq, France), was utilized as the nanometric reinforcement. It was supplied directly in the form of masterbatch, consisting of MWCNT dispersed in a thermoplastic matrix. For confidentiality reasons, the specific designation of the carrier resin has not been disclosed. According to the thermogravimetric analysis (TGA) certificate, the MWCNT mass concentration is

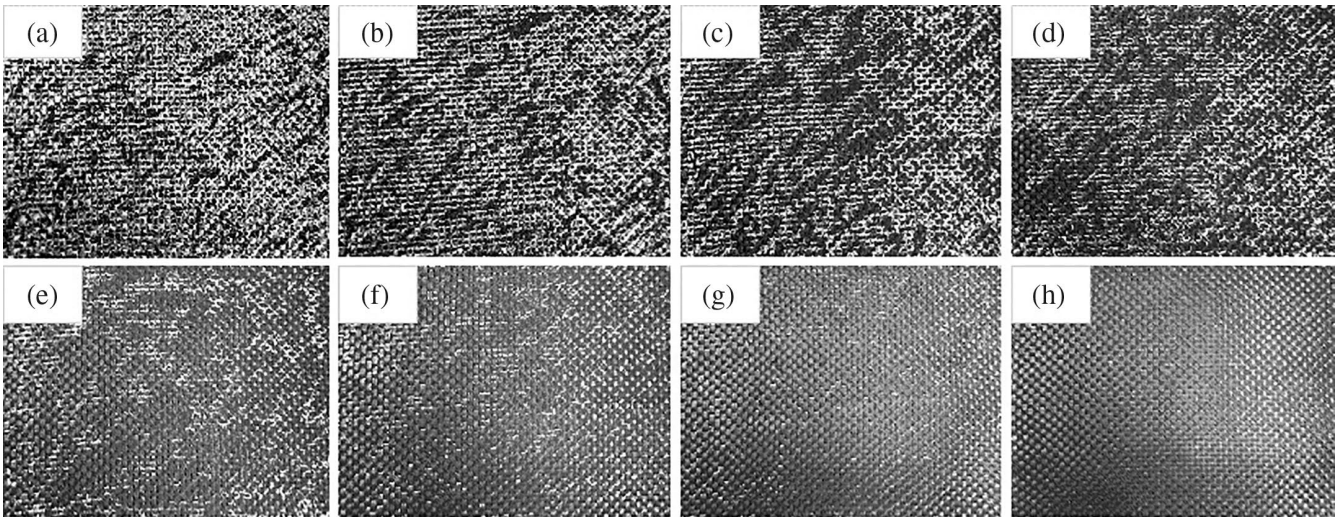

FIGURE 1 | Impregnated glass fabrics at various MWCNT contents, (a) 0.5 wt%, (b) 1 wt%, (c) 1.5 wt%, (d) 2 wt%, (e) 2.5 wt%, (f) 3 wt%, (g) 3.5 wt%, and (h) 4 wt%.

4.5 ± 0.2 wt% and the mass ratio after drying for 1 h at 125°C is about 6.0 ± 0.2. The MWCNT density is ranging between 1and $-1.65\,g/cm^3$, it exhibits a very high Young's modulus of approximately 1000 GPa and a Poisson ratio ranging between 0.2 and 0.3. In the reminder of this manuscript, the shortened term Graphistrength will be preferred.

2.2 | Processing

The glass fiber/Elium acrylic laminates containing MWCNTs were manufactured at the IRT M2P Composite Park site (Porcelette, France). The laminate composites were fabricated using a vacuum resin infusion process to impregnate the glass fiber woven, following a methodology similar to that described in the literature [42]. Initially, a direct infusion process of the Elium acrylic resin mixed with MWCNTs into the glass fiber woven was attempted; however, significant nanoparticle filtration issues occurred within the fabric layers. To overcome this limitation, a hybrid approach was adopted: a precise amount of MWCNT masterbatch was manually preimpregnated onto both faces of each glass fiber woven layer prior to the final vacuum infusion step (as illustrated in Figure 1). The manufacturing of the hybrid laminates-consisting of four woven glass fiber layers with dimensions of 390 mm × 390 mm, involved three distinct steps. First, during the formulation step, the volume of Graphistrength was determined based on the targeted weight fraction (wt%) of MWCNTs. Second, the preimpregnation step involved the manual coating (hand lay-up) and subsequent drying of the woven glass fiber layers. Finally, during the infusion step, the assembly of four preimpregnated woven glass fibers was subjected to the final vacuum resin infusion with pure Elium acrylic resin.

2.2.1 | Determination of Graphistrength Volume for Impregnation

The volume of Graphistength was calculated based on the dilution relation (1) which defines the mass balance between the solute (Graphistrength) and a solvent (Elium E151). Considering the initial weight fraction of MWCNT in Graphistrength (Cm_1) and the targeted weight fraction in the final E151 resin (Cm_2), the dilution relation is expressed as follows:

$$Cm_1 \times V_1 = Cm_2 \times V_2 \tag{1}$$

where (V_1) and (V_2) denote the volume of Graphistength and E151 OSA resin, respectively. Using Expression (1), the main objective was to determine the required volume (V_1). For this purpose, the weight fraction Cm_2 was fixed, while the volume (V_2) was determined based on the specifications of laminate composite plate. The volume (V_2) is considered equivalent to the volume of the laminate matrix after polymerization, which can be calculated using the following expression:

$$V_2 = \frac{m_e}{\rho_e} \tag{2}$$

where m_e and ρ_e denote the mass and density of the laminate matrix, respectively. The mass (m_e) can be obtained from the volume fraction of the glass fibers (f_f) within the laminate composite. Considering the resin infusion process, the volume fraction (f_f) is approximately 55%, as reported in the literature [1]. By neglecting the presence of porosities and voids within the laminate composite, the volume fraction (f_f) can be defined as follows:

$$f_f = \frac{V_f}{V_f + V_2} \tag{3}$$

where V_f denoted as the volume of glass fibers. Considering the mass (m_f) and the density (ρ_f) of the glass fibers, the volume V_f can be determined by:

$$V_f = \frac{m_f}{\rho_f} \tag{4}$$

Thus, combining Expressions (2) and (4), the volume fraction (f_f) takes the following form:

$$f_f = \frac{m_f \times \rho_e}{m_f \times \rho_e + m_e \times \rho_f} \tag{5}$$

TABLE 1 | Determination of Graphistrength volume according to the MWCNT content.

MWCNT (wt%)	0	0.5	1	1.5	2	2.5	3	3.5	4
m_f (g)	448.5	448.8	451.1	452.9	454.3	455.5	458.5	460.1	464.6
m_e (g)	169.1	169.3	170.1	170.8	171.3	171.8	172.9	173.5	175.2
V_2 (mL)	143.3	143.4	144.2	144.7	145.2	145.6	146.5	147.0	148.5
V_1 (mL)	—	16.7	33.5	50.5	67.5	84.6	102.2	119.7	138.1

Finally, the mass of the laminate matrix (m_e) can be expressed as follows:

$$m_e = \frac{m_f \times \rho_e}{\rho_f}\left[\frac{1}{f_f} - 1\right] \quad (6)$$

Using the Expression (6), the weight of glass fibers (m_f) remains the only unknown variable, which was directly obtained by weighing the four glass fabric layers of the laminate composite. Once the mass (m_e) was calculated, the volumes (V_1) and (V_2) were determined using the Relations (2) and (1), respectively, based on the selected MWCNT content (Cm_2) in the laminate composite. As noted above, the initial mass concentration of MWCNT (Cm_1) was approximately 4.5 ± 0.2 wt%. However, calculations utilizing Expression (6), indicating that the resultant volume of the masterbatch was insufficient to facilitate the manual impregnation of both sides of each glass fiber layer. To overcome this limitation, a larger baseline quantity of Graphistrength were prioritized; thus, height weight fractions of MWCNT ranging from 0.5 to 4 wt% were considered. The 0.5 wt% increment ratio was selected not only to facilitate manual impregnation by providing sufficient material volume for each side of glass fabrics, but also to evaluate the sensitivity and accuracy of the resulting material properties. Table 1 summarizes all the values obtained from the aforementioned expressions. Additionally, the laminate composite reinforced with neat MWCNT was also included as a control baseline for comparison.

2.2.2 | Impregnation of the Glass Fabrics

The glass fabric layers were manually preimpregnated in the Laboratory for the Study of Microstructures and Mechanics of Materials (LEM3), Metz, France. One-eighth of the total calculated volume V_1 (as detailed in Table 1) was allocated to each side (front and back) of the individual glass fabric layers. To ensure a highly uniform distribution of nanoparticles across the reinforcement phases, several processing precautions were strictly observed. First, the woven glass fiber layers were cut to identical dimensions of 390 mm × 390 mm to guarantee that an identical quantity of Graphistrenth MWCNTs was applied to each face, with mass measurement prioritized over volume measurement to achieve superior accuracy. Second, the Graphistrenth MWCNT masterbatch was delicately and systematically applied using a plastic spatula, layer by layer and side by side, until the entire surface area was completely and evenly covered, requiring an impregnation process of approximately 1 h per side. Finally, strict contamination control was maintained by thoroughly cleaning both the mixing beaker and the application spatula after completing the impregnation of each individual side. Following the preimpregnation process, each assembly of four coated glass fabrics was dried at 70°C for 8 h in a WTB Binder drying oven prior to the final vacuum resin infusion. Figure 1 illustrates the resulting color gradient and shade variations obtained for each specific MWCNT content.

2.2.3 | Vacuum Resin Infusion

The vacuum resin infusion process was performed in three distinct steps, as illustrated in Figure SI-1. First, during mold preparation and lay-up assembly, the infusion worktable surface was thoroughly cleaned and coated with a release agent before four plies of preimpregnated glass fabric, cut to dimensions of 390 mm × 390 mm, were stacked and aligned in a matching $[0/90]_4$ orientation (warp-on-warp and weft-on-weft, respectively). This stacked assembly was successfully covered with a release film and a distribution media (draining grid), and a vacuum bag was placed over the entire setup and hermetically sealed to the worktable using tacky tape (mastic sealant). Second, during resin degassing and modification, the base Elium resin was degassed using a vacuum chamber setup operating at a stirring speed of 450 rpm under a reduced pressure of 250 mbar for 15 min, at which stage the initial E150 resin was modified into the final E151 resin system optimized for the infusion of the hybrid MWCNT laminates. Third, during infusion and postcuring, the pressure within the sealed vacuum bag enclosure was verified to be approximately 4 mbar to ensure no leaks were present before a peroxide catalyst (Butanox M-50) was thoroughly mixed into the prepared resin matrix. The vacuum resin infusion was subsequently executed at room temperature (20°C) under a controlled driving pressure of 100 mbar, infusing four laminate plates simultaneously for each targeted MWCNT concentration utilizing a centralized resin feed point. Finally, the finished laminate composite plates were demolded approximately 1 h after the completion of the infusion and subjected to a postcuring cycle at 70°C for 8 h in a convection oven to guarantee full polymerization and cross-linking. The control laminate composite consisting purely of glass fiber woven and Elium resin was designated as E151/GF. The hybrid laminates were labeled systematically according to their specific MWCNT weight fractions. Thus, for the concentrations of 0.5, 1, 1.5, 2, 2.5, 3, 3.5, and 4 wt%, the reinforced laminate composites are designated as follows: E151MWCNT0.5/GF, E151MWCNT1/GF, E151MWCNT1.5/GF, E151MWCNT2/GF, E151MWCNT2.5/GF, E151MWCNT3/GF, E151MWCNT3.5/GF, E151MWCNT4/GF.

3 | Characterization

3.1 | Resin Diffusion Test

A resin diffusion test was performed directly on the worktable during the vacuum resin infusion process.

This test aimed to evaluate how the manual preimpregnated of the glass fabrics affected the flow and diffusion of the resin through the layout assembly. During vacuum resin infusion, two distinct diffusion fronts can be identified [43], as illustrated for the neat MWCNT-reinforced laminates in Figure SI-2. Relative to the initial reference position and following the flow direction, the first diffusion level occurs between the draining grid and the upper glass fabric layer; this primary front highlights the evacuation of residual air bubbles trapped within both the liquid resin and the dry glass fibers. The second diffusion level encompasses all four glass fabric layers simultaneously, thereby representing the actual bulk resin flow front. Consequently, this second front was selected as the metric for the diffusion test. To accurately track the flow propagation, four operators were positioned around the infusion worktable. Depending on the flow direction, the distance traveled by the resin through the woven glass fibers was recorded every 10 s, by marking the advanced fluid front directly onto the vacuum bag with a marker (as illustrated in Figure SI-1). These measurements were taken across a total span of 330 mm and the average distance covered was calculated for each time increment. To achieve statistical reliability, eight samples were tested for each specific MWCNT concentration.

3.2 | Microstructures

Microstructural analyses were conducted in two steps. First, the dispersion state of MWCNTs and the arrangement of the glass fibers were evaluated using an environmental scanning electron microscope (SEM, FEI Quanta FEG 250), available at LEM3 laboratory (Metz, France). For each laminate composite configuration, five specimens with dimensions of $10\,\text{mm} \times 10\,\text{mm} \times 2.3\,\text{mm}$ were extracted using water jet cutting equipment. The samples surfaces were manually polished using abrasive papers with successive grit sizes of 15, 10, 8, and 5 μm. Subsequently, ion beam polishing was carried out under the following operating conditions: a beam angle of 3°, an acceleration voltage of 5.5 keV, and an exposure time of 1 h per sample. Second, the same polished samples were subjected to atomic force microscope (AFM) analyses to gain high-resolution insights into the nanoscale dispersion of the MWCNTs within the polymer matrix. Thus, the atomic force analyses, supplied by LEM3 laboratory (Metz, France), were carried out on an AFM (Dimension Icon, Bruker) operating in Peak Force Quantitative Nanomechanical Mapping (PFQNM) mode. In this study, porosities have not been studied.

3.3 | Tensile Tests

Tensile tests were conducted at the mechanical characterization laboratory of National School of Arts and Crafts (ENSAM), Metz, France. All mechanical evaluations were performed at room temperature (20°C) under quasi-static loading conditions using an MTS 20/M universal testing machine equipped with a 100 kN maximum load cell. In compliance with the ISO 527-4 standards, rectangular specimens with nominal dimensions of $250\,\text{mm} \times 25\,\text{mm} \times 2.3\,\text{mm}$ were extracted from the laminate plates using waterjet cutting. All specimens were oriented at [0/90] principal axes and tested at a constant crosshead displacement speed of 1 mm/min, which corresponds to a quasi-static strain rate of $1 \times 10^{-4}\,\text{s}^{-1}$. Longitudinal and transverse strains were recorded simultaneously using a clip-on multiaxis extensometer (MTS model 632.85F-05) to accurately determine the elastic constants. For statical reliability, an average of 10 replicate specimens were tested for each laminate composite configuration.

3.4 | Low-Velocity Impact Tests

Low-velocity impact testing was conducted to evaluate the damage resistance of a fiber-reinforced polymer matrix composite subjected to drop-weight impact event. In accordance with the ASTM D7136/D7136M standard (an internationally recognized testing protocol developed by the ASTM International organization.). The procedure determines the damage resistance of multidirectional, continuous-fiber-reinforced polymer matrix composite plates subjected to a low-velocity, out-of-plane drop-weight impact. The experiments were performed using the Zwick/Roell Amsler HIT 2000F drop tower device at the Institute of Fundamental Technological Research of the Polish Academy of Sciences, Pawinskiego (Warsaw, Poland). Square specimens with nominal dimensions of $100\,\text{mm} \times 100\,\text{mm} \times 2.3\,\text{mm}$, extracted from the laminate plates via waterjet cutting, secured within the test fixture enclosure using a four point clamping configuration [44]. The drop height was adjusted based on the total mass of the impactor photocell system (approximately 10.1 kg) to achieve the target impact energies. The incident velocity of the impactor immediately prior to contact was recorded by an integrated photocell system, which simultaneously triggered an automated anti-bounce mechanism to prevent secondary impacts. A high-speed camera records the Kinematic profile of the hemispherical impactor tip, which featured a diameter of 16 mm. The impact tests were carried out at room temperature (20°C) under four distinct energy levels: 10, 20, 40, and 60 J. For each specific laminate composite configuration, an average of three replicate specimens were tested to ensure statical repeatability.

3.5 | Electrical Conductivity

Dynamic Dielectric measurements were conducted using a Novocontrol Broadband Dielectric Spectroscopy apparatus equipped with an Alpha Analyzer and a Quattro temperature controller (BDS 1330), at Jean Lamour Institute (IJL), Nancy, France. The measurements were performed at room temperature (20°C) over a broad frequency range spanning from 0.5 to 10^6 Hz. Square specimens with nominal dimensions of $25\,\text{mm} \times 25\,\text{mm} \times 0.9\,\text{mm}$. The specimens were subsequently polished manually using 15 μm grit abrasive paper until a uniform target thickness of 0.9 mm was achieved. The out-of-plane (through-thickness) electrical conductivity was measured by placing the samples between two gold-plated parallel-plate electrodes featuring a diameter of 20 mm. The dielectric measurement configuration and protocol were

executed through a systematic sequence of steps. First, the polished samples were sandwiched between gold-plated electrodes to establish optimal electrical contact. Next, the electrode-sample assembly was mounted inside the test cell, and a controlled, uniform contact pressure of approximately 5 N was applied to minimize interfacial contact resistance and eliminate capacitive air-gap artifacts. A sinusoidal AC voltage with an amplitude of 1 V was then applied across the thickness of the sample to generate a stable alternating electric field. Finally, prior to running the experimental matrix, the system was fully calibrated against standard reference materials supplied by Novocontrol to eliminate systematic phase and impedance errors. The complex dielectric permittivity (ε^*), real permittivity (ε'), dielectric loss (ε''), Dielectric loss tangent (tan δ) and AC conductivity (σ_{AC}) were extracted and processed using WinDETA software. For each specific laminate composite configuration, an average of three replicate specimens were analyzed to ensure statical repeatability.

4 | Results and Discussion

4.1 | Resin Diffusion

Figure 2 illustrates the resin diffusion profiles as a function of time, revealing two distinct fluid propagation phases. Between the initial measurement times of 10–20 s, the resin advanced rapidly, achieving a high initial flow front velocity that covered a distance of approximately 60 mm. Beyond 20 s, the diffusion rate slowed significantly, stabilizing at a steady-state average incremental advancement of approximately 25 mm. Across all measurement increments, the resin flow front velocity globally decreased as the MWCNT concentration within the laminate composite increased. Consequently, a higher carbon nanotube content led to a systematically retarded resin diffusion profile. The flow retardation is particularly pronounced for the 3.5 and 4 wt% MWCNT concentrations at every recorded time step. Thus, the addition of MWCNTs introduces a distinct resistance to resin diffusion, compounding the inherit tortuosity of the yarn network which traditionally restricts resin flow. This effect would not only be due to the increased

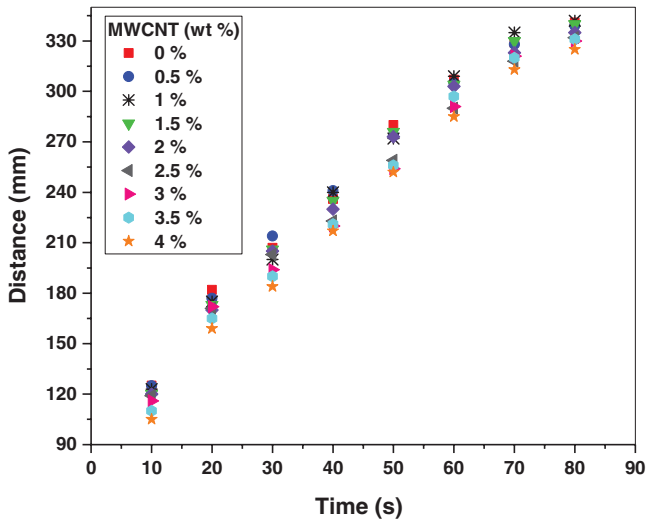

FIGURE 2 | Resin diffusion graph of MWCNT-based laminate composites.

of MWCNT content, but also to the hand layup impregnation of glass fiber woven. Indeed, with increasing MWCNT content, the glass fiber woven became completely covered with Graphistrenth, and hand layup impregnation did not allow a uniform distribution on the fibers. Furthermore, stacking four successive glass fabrics could cause particles aggregates at yarn interfaces, creating obstacles to resin diffusion in certain regions. Figure 1 clearly illustrates the likelihood of aggregate particle regions on glass fiber woven. Fundamentally, the introduction of MWCNT alters both the macro-permeability of the fiber preform and the molecular mobility of the fluid matrix. During the vacuum infusion process, the liquid resin must migrate smoothly through the porous glass fiber network, which acts as a filter. Due to the highly viscous nature of the Graphistrength masterbatch and its nonuniform local dispersion, large nanotube clusters dramatically reduce the effective permeability of the medium, thereby slowing down the flow-front progression. Furthermore, at the micro-atomic scale, the rigid structures of the nanotubes interact directly with the advancing polymer chains. The physical presence of well-entangled carbon nanotubes creates severe steric hindrance, forcing the resin's polymer pathways into a highly tortuous route. This restricts local molecular chain movement, leading to a significantly depressed diffusion coefficient compared to the pure resin system. Finally, the decrease in diffusion velocity observed after 20 s is also a result of the simultaneous infusion of four laminate composites, as shown in Figure SI-1. Using a centralized infusion point establishes a balanced resin distribution across all four plates, as observed at a diffusion level of 180 mm.

4.2 | MWCNT Dispersion

Figure 3 shows the microstructure of the E151MWCNT2/GF laminate composite obtained via SEM and AFM analyses. As shown in the SEM micrograph (Figure 3a), direct observation of individual carbon nanotubes was limited at this scale; however, the imaging clearly revealed nanoparticle-dense and nanoparticle-depleted regions of Graphistrength concentrated at the yarn interfaces, a morphology consistent across all modified laminates. Despite the resolution limits regarding individual carbon nanotubes, the geometric dimensions of the glass fiber woven architecture were successfully quantified from the SEM data. The yarn cross-sections exhibited a characteristic elliptical geometry, with major and minor axes ranging from 4.51 to 5.20 mm and from 0.49 to 0.61 mm, respectively. Additionally, the individual glass fibers exhibited a mean diameter of 17.07 μm with a standard deviation of 1.56 μm. In contrast to the SEM observations, AFM images provided significantly higher resolution and precision regarding the local dispersion state of Graphistrength masterbatch. Figure 3b shows the less rich area of Graphistrength, which appears as grooves oriented in the same oblique direction. Various groove sizes with asperities were observed along with denser zones. In contrast, the rich area of Graphistrength shown in Figure 3c, revealed aggregate particles visible at a magnification of 1 μm. Some regions appeared denser, while others were porous.

Consequently, these microstructural evaluations confirm a nonuniform dispersion of Graphistrength throughout the bulk composite material, mirroring the trends observed in the other reinforced laminate variants. Notably, these localized particle agglomerations became progressively more pronounced and

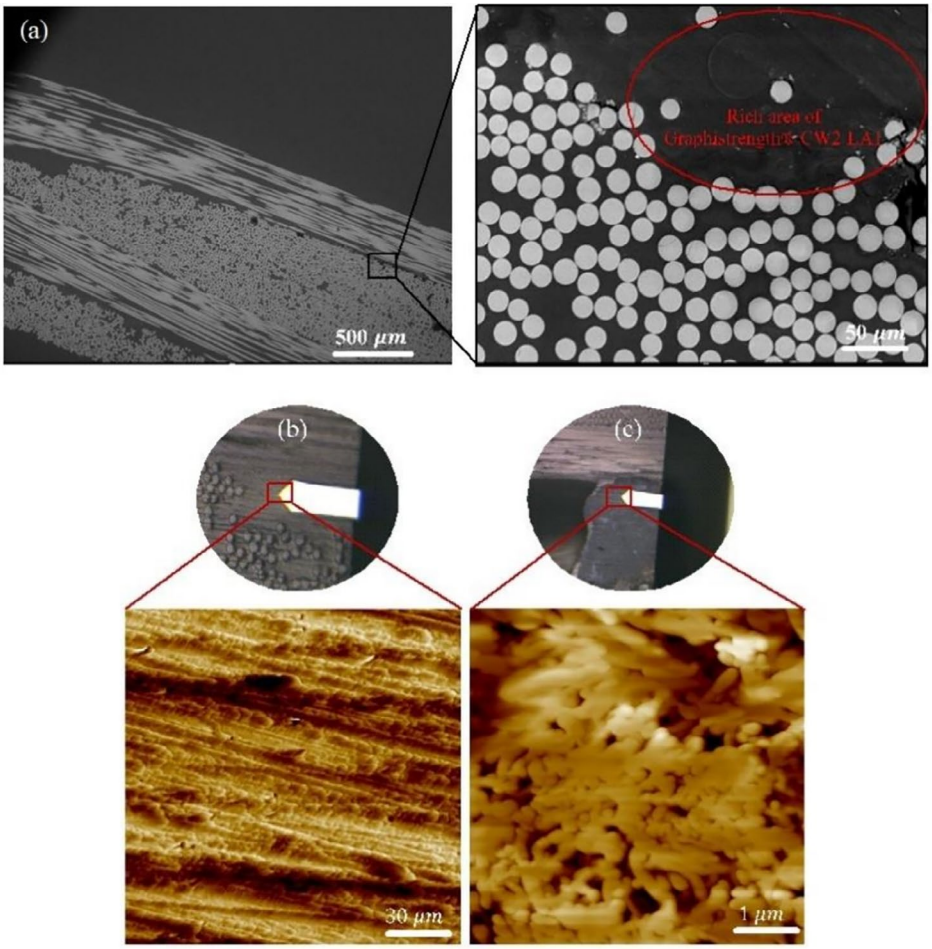

FIGURE 3 | Microstructure of E151MWCNT2/GF laminate composite: (a) dispersion state of glass fibers, (b, c) less-rich and rich areas of Graphistrength.

visible at the interply yarn interfaces beyond an MWCNT content of 2 wt%.

As shown in Figure 3, the final dispersion state of MWCNTs is partly governed by the nature of the Graphistrength masterbatch, which inherently contains localized agglomerates resulting from its primary synthesis and preparation process. Consequently, particulate aggregates of MWCNT are commonly observed within the composite microstructures, even at low mass fractions [45, 46] and even after dilution in another solution or resin [47, 48]. According to Arkema's technical specifications, the MWCNT are initially well dispersed within the masterbatch carrier; therefore, the dispersion morphology highlighted in Figure 3 is likely an artifact during the manual hand-impregnation protocol. In addition to the laminate processing challenges detailed previously, the characteristically high aspect ratio and structural tortuosity of the MWCNTs could lead to localized filtering phenomena as the resin migrates through the tight fiber gaps.

Furthermore, the pasty consistency of the masterbatch may also have contributed and should not be overlooked. Such dispersion can affect the expected mechanical properties since good dispersion of nanoparticles ensures good performance [10]. The specific impacts of this MWCNT dispersion state on the resulting elastic properties of the laminates are detailed systematically in the following section.

4.3 | Elastic Properties

Figure 4 shows the representative nominal stress–strain curves of the laminate composites tested along the weft direction. The curves exhibit approximately similar linear region followed by a nonlinear one, but differences can be distinguished at the elongation at break. In the weft direction, the nominal stress decreased from 405.4 for the E151/GF to 309.2 MPa, E151MWCNT0.5/GF laminate. This represents a 23.7% reduction in stress, while alongside 14.5% drop in the elongation at break. However, beyond this initial 0.5 wt% threshold, both the nominal stress and ultimate strain increased progressively with higher MWCNT content, reaching a peak at a concentration of 2.5 wt%. At this optimal configuration (E151MWCNT2.5/GF), the nominal stress and strain reached 424.9 MPa and 0.059, respectively, corresponding to a 4.6% increase strength and a 6.8% increase in elongation compared to the baseline E151/GF. Regarding the elastic modulus, the modulus increased with the MWCNT addition, raising from a value of 22.24 GPa to a maximum value of 25.2 GPa at 2.5 wt%. This peak represents a 13.3% enhancement relative to E151/GF. Beyond 2.5 wt% of MWCNT content, the

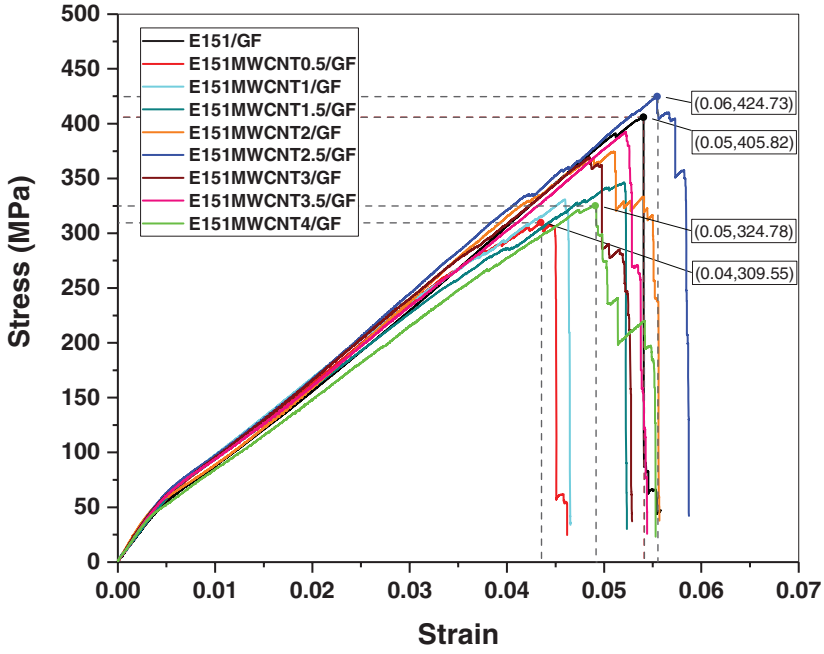

Loading rate	Tensile properties	MWCNT content (wt %)								
		0	0.5	1	1.5	2	2.5	3	3.5	4
1 mm/min (Weft direction)	Young Modulus E_{22}(GPa)	22.24 ±0.69	22.98 ±0.67	24.16 ±0.65	24.49 ±0.75	24.88 ±0.78	25.20 ±0.67	23.55 ±0.83	23.20 ±0.88	23.19 ±0.67
	Maximal stress σ_{22}^{r}(MPa)	405.45 ±14.26	309.21 ±24.05	330.54 ±20.67	345.72 ±7.95	374.43 ±22.18	424.87 ±26.76	365.34 ±16.06	392.29 ±18.79	324.78 ±19.92
	Elongation at break A_{22}^{r}%	0.055 ±0.001	0.047 ±0.004	0.045 ±0.002	0.046 ±0.001	0.051 ±0.001	0.059 ±0.001	0.051 ±0.002	0.053 ±0.001	0.050 ±0.001
	Poisson ratio ν_{12} (-)	0.21 ±0.001	0.2 ±0.002	0.19 ±0.001	0.18 ±0.001	0.18 ±0.003	0.16 ±0.005	0.16 ±0.002	0.12 ±0.005	0,13 ±0.001
1 mm/min (Warp direction)	Young Modulus E_{11}(GPa)	26.93 ±0.88	28.64 ±0.93	31.60 ±0.55	31.30 ±0.98	31.87 ±0.61	30.27 ±0.48	29.18 ±0.67	27.52 ±0.73	26.87 ±0.59
	Maximal stress σ_{11}^{r}(Mpa)	480.09 ±09.11	459.22 ±13.65	487.83 ±06.24	510.01 ±14.57	523.12 ±10.89	501.34 ±15.47	465.31 ±08.74	464.27± 12.02	432.25 ±05.36
	Elongation at break A_{11}^{r}%	0.055 ±0.001	0.056 ±0.002	0.060 ±0.001	0.059 ±0.002	0.061 ±0.002	0.059 ±0.003	0.057 ±0.001	0.055 ±0.002	0.054 ±0.001
	Poisson ratio ν (-)	0.21 ±0.001	0.20 ±0.001	0.20 ±0.003	0.19 ±0.002	0.19 ±0.001	0.19 ±0.003	0.18 ±0.001	0.16 ±0.002	0,15 ±0.002

FIGURE 4 | Tensile properties of MWCNT reinforced laminate composites at a loading rate of 1 mm/min.

Young's modulus gradually decreased but consistently remained higher than that of E151/GF. For instance, the E151MWCNT4/GF laminate exhibited a modulus of 23.19 GPa which is approximately 4% higher than that of E51/GF. Concurrently, the Poisson's ratio, exhibited a slight, gradual decrease with the increasing MWCNT content. The elastic properties in the both warp and weft directions globally followed identical trends, except to their values. As shown in Figure 4, the E151/GF laminate exhibited a Young's modulus of 26.93 GPa in the warp direction, which is roughly 21% higher than its corresponding value in the weft direction. Furthermore, in the warp direction, the peak Young's modulus reached 31.87 GPa at a slightly threshold of 2 wt% of MWCNT content, yielding an 18% improvement over the E151/GF. Similarly, the nominal stress reached a maximum enhancement of approximately 9% at this same 2 wt% MWCNT concentration relative to E51/GF.

The increase of Young modulus can be attributed to the inherently high Young's modulus of MWCNT, as reported in the literature [13, 49]. As noted by Nadeem M. et al. [15], the Young modulus of MWCNT, which is approximately 1 TPa, provides strong reinforcement and improves composite stiffness. This improvement also results from good dispersion and orientation of MWCNT at moderate weight fractions (0.5–2.5 wt%), as reported by Fulmali et al. [22]. MWCNT contribute positively to tensile and flexural properties, depending on nanotube characteristics such as type, purity, aspect ratio, concentration, orientation, dispersion state, and the polymer matrix [16]. MWCNT with very high aspect ratio (100 – 1000) provide numerous bonding sites due to their multiwall structure [22, 23]. Moreover, the specific laminate processing protocol likely contributed to the enhancement of elastic properties. In practice, the manual hand layup impregnation of the glass fabric allowing the carbon

nanotubes to adhere closely to the glass fiber surfaces, This close physical proximity enhances the interfacial fiber-matrix adhesion, through mechanical interlocking and local stress-transfer paths, a mechanism consistent with the findings reported by Dheepthi et al. [24]. MWCNT-grafted fibers exhibited significantly enhanced interfacial shear strength due to improved wettability [16, 50]. Strong fiber–matrix adhesion combined with the high aspect ratio of MWCNT increase the load-bearing surface area, enabling better stress transfer from the Elium matrix to the fibers [28, 29, 51]. Thus, the performance observed in Figure 4 could be attributed to the robust interfacial bonding established between glass fibers and MWCNT. At a low concentration of 0.5 wt% MWCNT, the nominal stress and the elongation at break decreased by 23.7% and 14.5% compared to E151/GF, respectively. This localized degradation in ultimate properties can be explained by the initial dispersion state resulting from the manual hand lay-up processing. Although the high modulus of the MWCNTs successfully increased the overall Young's modulus, insufficient Graphistrength coverage at low concentrations led to highly heterogeneous nanoparticle distribution at the yarn interfaces. These regions formed stress concentration zones that disrupting composite continuity, causing premature macro-scale failure. Conversely, increasing the MWCNT content optimized interfacial adhesion which subsequently enhanced both the ductility and the stress of the composite. The surface textures observed within the 2–2.5 wt% range (as shown in Figure 1e) confirm this improved, highly uniformed distribution of MWCNTs on the woven glass fiber. Beyond 2.5 wt% of MWCNT content, the decrease in Young's modulus could be attributed to MWCNT aggregates in the microstructure [36, 52], as shown in Figure 3. Aggregates may reduce matrix-fiber contact areas and act as stress concentrators rather than transmitters [53], leading to poor interfacial bonding and lowering mechanical properties [36, 54]. As shown in Figure 3a,b, some aggregates regions were already present at 2 wt% of MWCNT content. Therefore, when the MWCNT content exceeded 2.5 wt%, aggregates would become more prevalent and that could explain the decrease in elastic properties. Additionally, some porosities were observed from 2 wt% MWCNT. In this study, porosities were not studied, but they could further lead to weak fiber–matrix bonding which could be reduce the composite's stiffness, as also reported by Dalina et al. [25].

The tensile stress–strain curve peaks at an optimal MWCNT concentration of 2 and 2.5 wt% in the warp and weft directions, respectively. These thresholds represent an ideal equilibrium between maximum mechanical reinforcement and the onset of processing-induced laminate defects. These optimal concentrations indicate highly efficient stress-transfer mechanics throughout the bulk composite assembly, which is likely facilitated by a globally uniform dispersion of the carbon nanotubes. When properly dispersed, the MWCNTs maximize their effective surface-area-to-volume ratio, thereby optimizing interfacial interactions with the surrounding polymer matrix. Consequently, applied mechanical loads are efficiently transferred from the more compliant resin matrix to the highly rigid carbon nanotubes networks, concurrently maximizing both the ultimate tensile stress and the elastic modulus.

Furthermore, polymer composite matrices are characteristically susceptible to micro-cracks when subjected to tensile loading. Within the 2–2.5 wt% concentration range of MWCNT content, the spatial density of the carbon nanotubes is sufficient to activate a distinct crack-bridging mechanism. In this regime, the nanotubes effectively span across advancing microcrack tips, anchoring the matrix together, restricting localized crack propagation, and ultimately delaying catastrophic macro-scale failure. Across all MWCNT concentrations, both the Young's modulus and nominal stress in the warp direction were systematically higher than those recorded in the weft direction. This directional variation is directly attributed to the high-volume fraction of glass fiber aligned along the warp direction, given that the mechanical properties and overall stiffness of a fiber-reinforced polymer composite are strongly dependent on the fiber volume fraction along the loading axis. Concurrently, the slight decrease observed in the Poisson's ratio indicates that the incorporation of MWCNTs effectively enhanced the lateral stiffness of the laminate composite, thereby restricting transverse deformation under axial tensile loading.

Furthermore, some observations can be made regarding the damage state of the tested specimens, as shown in Figure SI-3. When damage occurred, delamination areas were clearly observed in the laminate composites reinforced with MWCNT, compared to E151/GF composite. The higher the MWCNT content, the larger the delamination area, although not all layers failed simultaneously. The use of MWCNT as nanoscale reinforcement generally led to enhanced elastic properties of the laminate composites, especially the Young's modulus in this study. The increase of delamination intensity would likely reflect less good interlaminar bonding, probably due to the increase of MWCNT content in the laminate. For MWCNT-based laminate composites, at most two laminate layers were broken under tensile test, indicating strong resistance due to the addition of MWCNT. Even using in small quantities, MWCNT significantly enhance mechanical properties (stiffness, strength, toughness) compared to conventional composites [55], as well as the low-velocity impact properties.

4.4 | Low-Velocity Impact Properties

The impact behavior of laminate composites can be characterized by force–displacement and energy-time curves at various impact energies, as reported in the literature [3, 9]. Figure 5 shows the characteristic curves obtained at the impact energies of 10 and 20 J, and all the impact properties are reported in Table 2. At the impact energy of 10 J, the force–displacement curves (Figure 5a) follow a similar trend: a rise in force up to a peak, followed by a drop and ending with a low residual displacement. This trend generally indicates a moderate increase in peak force for all the composites reinforced with MWCNT, as well as the slight decrease in absorbed energy shown in Figure 5b. From Table 2, the E151MWCNT2/GF composite exhibits the lowest average absorbed energy of 4.1 J, while the highest average peak force of 4528.12 N is observed for the E151MWCNT1.5/GF composite.

At 20 J, the force–displacement curves (Figure 5c) show similar trends like those obtained at 10 J (Figure 5a), except for their peak forces and energies. Indeed, peak force increases with impact energy, as reported in the literature [4, 9]. In general, the properties of the MWCNT-reinforced composites remained higher

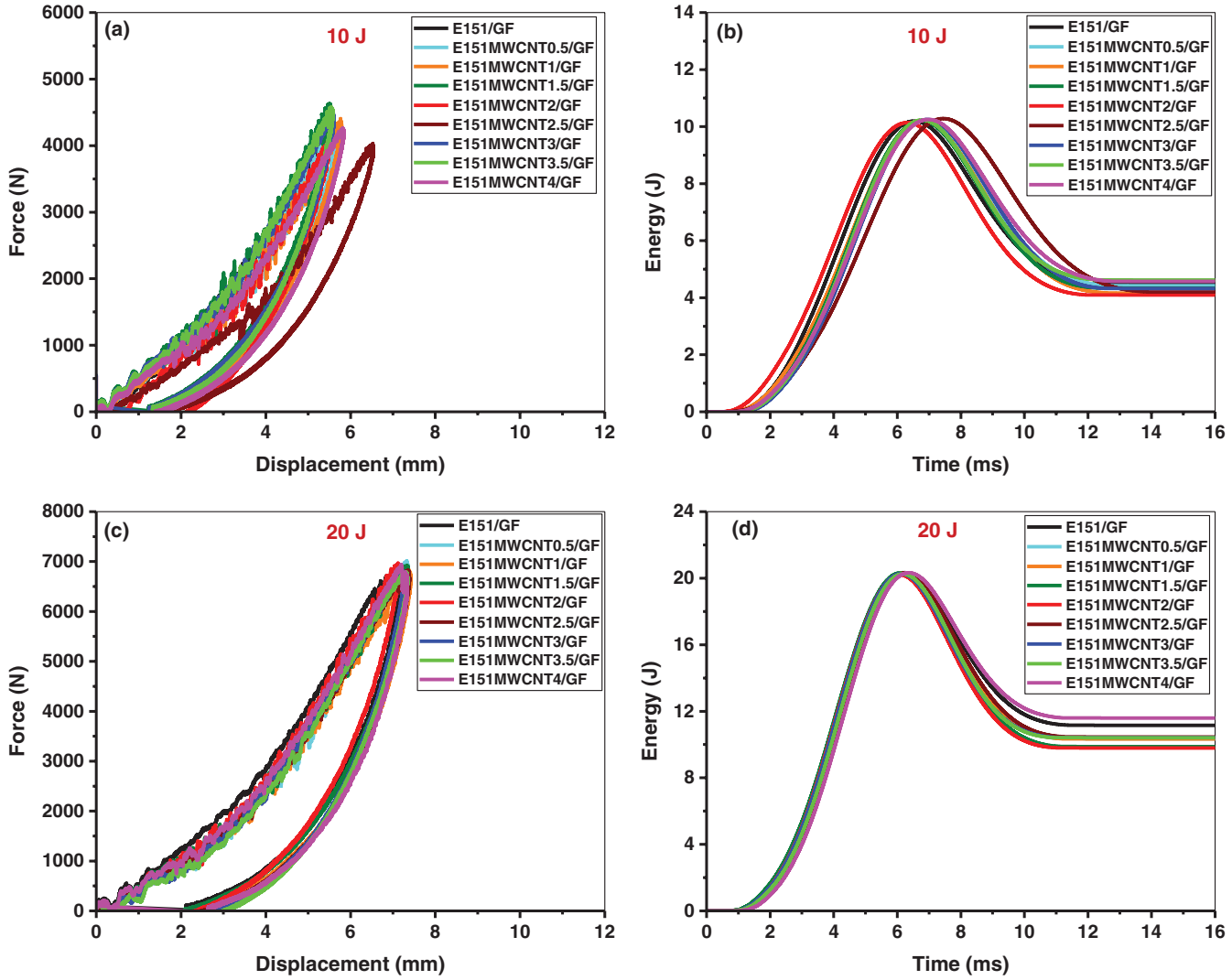

FIGURE 5 | Low velocity impact behavior of laminate composites, (a, b) force–displacement and energy-time curves at an impact energy of 10 J; (c, d) force–displacement and energy–time curves at an impact energy of 20 J.

TABLE 2 | Low velocity impact properties of laminate composites under impact energies of 10 and 20 J.

	10 J			20 J		
Laminate composites	E_a (J)	F (N)	D (mm)	E_a (J)	F (N)	D (mm)
E151/GF	4.37 ± 0.14	4330.91 ± 88.63	5.43 ± 0.01	10.95 ± 0.3	6881.97 ± 24.72	6.94 ± 0.15
E151MWCNT0.5/GF	4.47 ± 0.07	4391.28 ± 81.03	5.66 ± 0.03	10.47 ± 0.17	7062.45 ± 70.48	7.30 ± 0.04
E151MWCNT1/GF	4.41 ± 0.34	4477.91 ± 104.49	5.59 ± 0.25	11.22 ± 1.26	6707.17 ± 163.51	7.18 ± 0.29
E151MWCNT1.5/GF	4.33 ± 0.01	4528.12 ± 147.67	5.52 ± 0.02	10.01 ± 0.18	6854.83 ± 91.29	7.26 ± 0.09
E151MWCNT2/GF	4.09 ± 0.12	4233.52 ± 247.65	5.51 ± 0.08	9.80 ± 0.39	6849.01 ± 163.72	7.25 ± 0.18
E151MWCNT2.5/GF	4.28 ± 0.12	4201.88 ± 239.83	6.09 ± 0.62	11.19 ± 1.04	6865.11 ± 60.28	7.13 ± 0.31
E151MWCNT3/GF	4.38 ± 0.09	4355.03 ± 181.39	5.63 ± 0.05	10.45 ± 0.04	7028.10 ± 280.39	7.19 ± 0.03
E151MWCNT3.5/GF	4.64 ± 0.03	4391.59 ± 264.81	5.66 ± 0.16	10.92 ± 0.72	6939.94 ± 217.71	7.25 ± 0.11
E151MWCNT4/GF	4.56 ± 0.01	4294.66 ± 48.23	5.82 ± 0.01	11.63 ± 0.06	6682.48 ± 362.79	7.53 ± 0.47

than those of E151/GF composite. Notably, the highest average peak force of 7062.45 N was observed for E151MWCNT0.5/GF, indicating an increase of about 2.6% relative to E151/GF. E151MWCNT4.0/GF composite displays the lowest maximum force of 6682.48 N and a greater displacement of 7.53 mm, compared to all the composites.

As for the energy–time curves (Figure 5d), a more pronounced decrease in absorbed energy is observed for the MWCNT-reinforced composite, except to E151MWCNT4/GF. The last one absorbed more impact energy than E151/GF resulting from its low impact force. The lowest absorbed energy of 9.80 J was obtained for E151MWCNT2/GF composite. Considering the impact energies of 10 and 20 J, MWCNT-based laminate composites would show improved impact resistance, characterized by the higher peak forces and the lower absorbed energies. Moreover, E151MWCNT2/GF composite exhibited the best impact resistance, as it absorbed the least energy of all laminates. The small residual displacement ranging from 1 to 2.5 mm at the end of the force–displacement curves indicates that no penetration occurred in the laminate plates at the impact energies of 10 and 20 J, likewise in the literature [6, 9].

At impact energies of 40 and 60 J, more significant improvements in peak forces and absorbed energies were observed with MWCNT addition, as shown in Figure 6 and reported in Table 3. At 40 J (Figure 6a), the peak force of E151MWCNT2.5/GF composite was approximately 10 kN, representing an increase of more than 12%, compared to the control composite. As shown in Figure 6b, E151MWCNT1.5/GF composite exhibited the lowest absorbed energy of 26 J, corresponding to a decrease of 16.40%, compared to E151/GF.

At 60 J, the force–displacement and energy–time curves (Figure 6c,d) further confirmed the improved impact resistance due to MWCNT addition. The peak force of E151MWCNT0.5/GF composite increased by 15% over that of E151/GF, while the most significant reduction in absorbed energy of about 11% was observed for E151MWCNT1/GF. The energy–time curves also reveal that the penetration threshold was reached for E151/GF. Indeed, the absorbed energy of E151/GF nearly equaled the impact energy of 60 J, and the same composite exhibited the highest residual displacement of about 15.20 mm. Considering the impact energies of 40 and 60 J, E151MWCNT1.5/GF and E151MWCNT1/GF composites demonstrated better impact resistance, characterized by lower absorbed energies. The increase in impact resistance can also be attributed to strong fiber–MWCNT interfacial adhesion, promoted by hand impregnation of the glass fiber woven, as noted by Dheepthi et al. [24]. The high aspect ratio of MWCNT increases fiber engagement area and therefore improves stress transfer [28, 36]. Moreover, the high tortuosity of MWCNT creates a labyrinth-like structure that prevents damage propagation (matrix cracking, delamination, fiber breakage) [29].

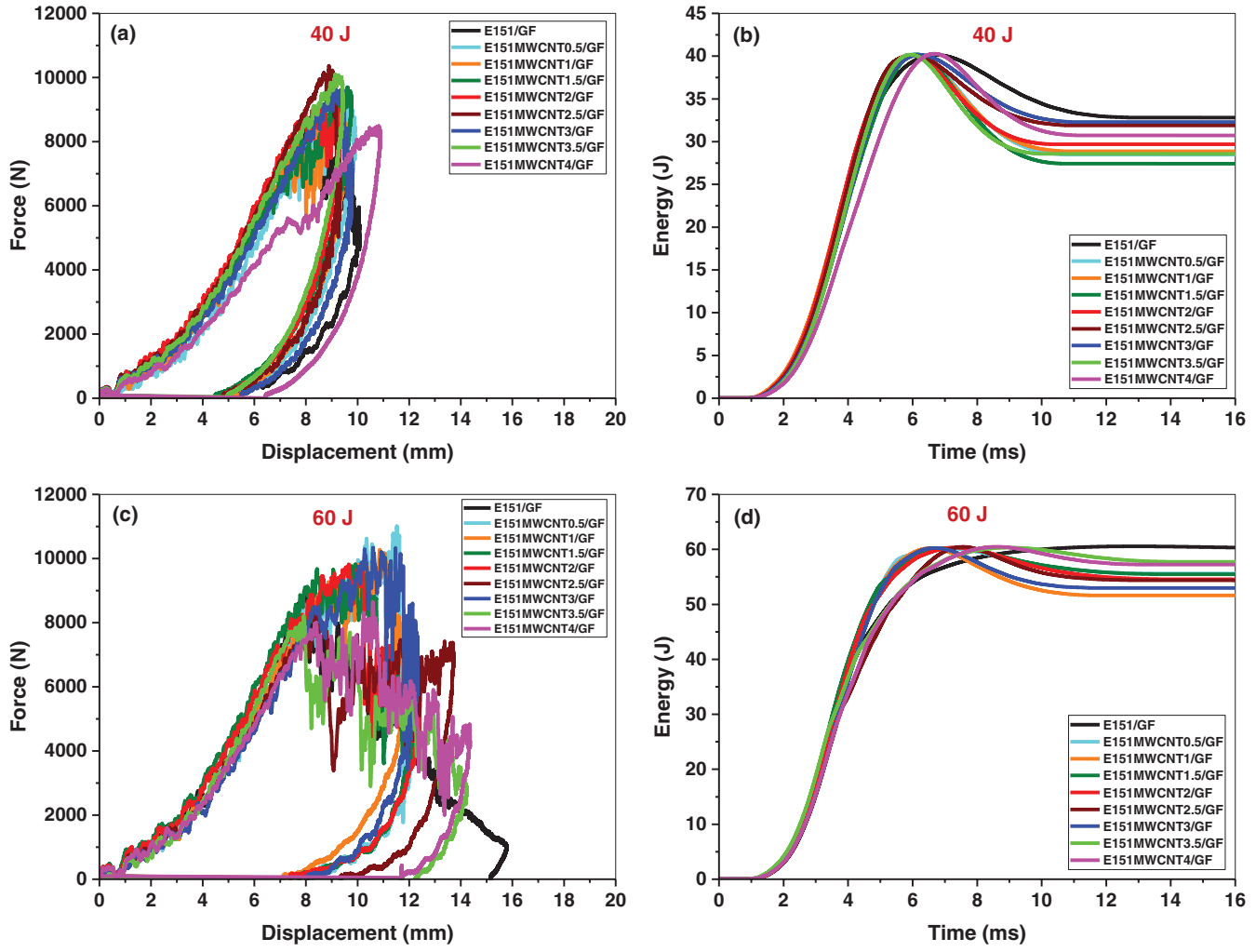

FIGURE 6 | Low velocity impact behavior of laminate composites: (a, b) force–displacement and energy–time curves at an impact energy of 40 J; (c, d) force–displacement and energy–time curves at an impact energy of 60 J.

Due to their high toughness [32, 56], MWCNT also help absorb impact energy, as reported by Grimmer and Dharan [30]. These improvements in impact energy also align with the penetration threshold analysis shown in Figure 7.

In addition to peak force and absorbed energy, the penetration threshold is one of the most common parameters used to assess the low velocity impact resistance of laminate composites, as reported in the literature [1, 6, 9]. According to the methods described by Aktas et al. [57] and Reis et al. [58], the penetration threshold can be determined by two approaches. First, the energy profile diagram (EPD), which plots absorbed energy as a function of impact energy, can be used. Thus, the penetration threshold is reached when the absorbed energy equals the impact energy. Second, the elastic energy can be plotted as a function of the impact energy and fitted with a second-degree polynomial. In this case, the penetration threshold corresponds to the nonzero root of the polynomial. In this study, the two methods described above were used to determine the penetration threshold of the laminate composites, as shown in Figure 7.

For lower impact energies of 10 and 20 J (Figure 7a), all the absorbed energies lie below the equal-energy line, and the effect of enhancing impact properties by adding carbon nanotubes is not visible enough. However, a clear difference appears from 40 to 60 J. All MWCNT-based laminate composites absorbed less energy than those without MWCNT, confirming earlier observations in Figure 6b,d. The absorbed energy of E151/GF composite lies on the equal-energy line at 60 J, while those of the other composites lie below it. It is clear that the penetration threshold of E151/GF composite is approximately 60 J, while those of the reinforced composites exceed 60 J. Thus, laminate composites based on MWCNT would be more resistant than the control composite, considering the impact energies of 40 and 60 J. These observations are confirmed by Figure 7b, of which the penetration threshold of E151/GF is about 59.2 J. Indeed, the penetration threshold increased with MWCNT addition, reaching a maximum of 76.65 J at 1 wt% of MWCNT content, then decreased to about 68.50 J at 2 wt%. The penetration threshold increased again to about 74 J at 3 wt% MWCNT content, before decreasing to 65 J. Up to 3 wt% MWCNT content, the reinforced composites

TABLE 3 | Low velocity impact properties of MWCNT-reinforced laminated composites under impact energies of 40 and 60 J.

	40 J			60 J		
Laminate composites	E_a (J)	F (N)	D (mm)	E_a (J)	F (N)	D (mm)
E151/GF	32.81 ± 1.75	8770 ± 221.19	7.94 ± 0.58	59.41 ± 1.22	9080.12 ± 12.47	8.65 ± 0.79
E151MWCNT0.5/GF	28.51 ± 0.07	9618.71 ± 10.84	9.32 ± 0.08	55.90 ± 0.54	10518.41 ± 692.29	10.79 ± 1.04
E151MWCNT1/GF	29.73 ± 1.19	9130.72 ± 78.61	9.08 ± 0.43	53.89 ± 3.22	9283.29 ± 1401.39	10.62 ± 0.33
E151MWCNT1.5/GF	27.43 ± 1.36	9445.06 ± 362.68	9.17 ± 0.62	55.04 ± 0.61	9944.17 ± 184.86	10.26 ± 0.48
E151MWCNT2/GF	29.99 ± 0.41	9121.14 ± 11.67	8.66 ± 0.15	54.87 ± 0.44	10285.72 ± 667.89	9.79 ± 0.19
E151MWCNT2.5/GF	32.43 ± 0.75	9806.17 ± 780.12	8.74 ± 0.23	55.01 ± 0.89	9059.79 ± 1153.63	9.16 ± 1.11
E151MWCNT3/GF	32.94 ± 0.91	9590.73 ± 106.79	9.22 ± 0.09	55.73 ± 3.88	9948.38 ± 544.29	9.47 ± 1.60
E151MWCNT3.5/GF	30.15 ± 2.22	9243.42 ± 1210.56	9.60 ± 0.66	57.51 ± 0.28	8890.09 ± 954.84	8.69 ± 1.08
E151MWCNT4/GF	30.47 ± 0.37	9210.92 ± 1020.39	9.83 ± 1.41	58.96 ± 2.46	8631.99 ± 9.76	9.99 ± 0.84

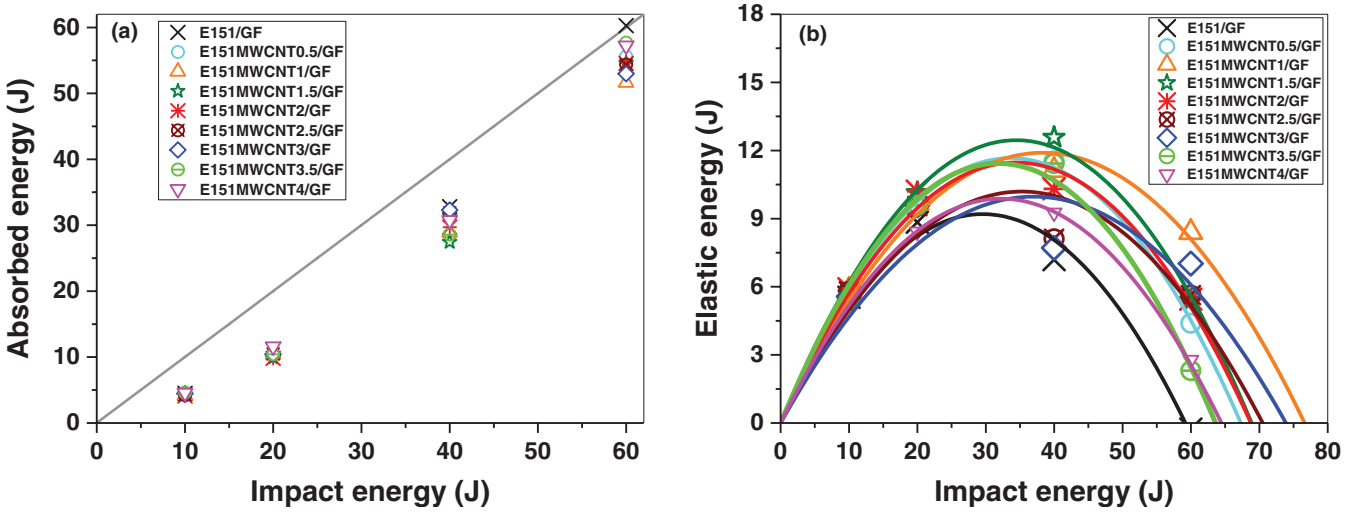

FIGURE 7 | Effect of MWCNT on the penetration threshold of laminate composites: (a) absorbed energy versus impact energy; (b) elastic energy versus impact energy.

exhibited the highest penetration thresholds, likely due to good MWCNT dispersion on the glass fibers. Beyond 3 wt% MWCNT (Figure 7), the penetration threshold decreased, likewise the tensile properties shown in Figure 4. This decrease was likely due to MWCNT aggregates, which reduce stiffness and strength by creating stress concentration within the laminate composite [25, 54]. However, all MWCNT-based laminate composites exhibited higher penetration thresholds than the control composite. Based on Figure 7b, E151MWCNT1/GF and E151MWCNT3/GF composites exhibited better impact performance. These findings are consistent with the illustration of Figure 8, in which the damage areas of E151/GF and E151MWCNT1/GF have been compared.

For impact energies of 10 and 20 J (Figure 8), all composites exhibited similar impact resistance and no penetration was observed, as well as it was observed in Figure 5a. At 40 J, the front side of E151/GF composite showed early penetration, unlike the composite containing 1 wt% MWCNT content. Differences between damage areas become more evident at 60 J, when the impactor clearly penetrated both faces of E151/GF. At the same energy, E151MWCNT1/GF showed no penetration marks, confirming that its ultimate resistance exceeds 60 J. The superior performance of E151MWCNT1/GF in terms of impact resistance represents an improvement of about 30%, compared to the E151/GF.

Notably the penetration threshold achieved here at a low concentration of 1 wt% MWCNT is higher than several comparable thresholds reported in the literature [9]. For context, previous studies investigating the effect of ambient conditions on impact resistance reported an optimal penetration threshold of approximately 62 J at −80°C, which was achieved using glass fibers reinforced with a significantly higher concentration of block copolymers (15 wt%). Furthermore, a glass fiber reinforced with 10 wt% of an acrylonitrile butadiene styrene ABS copolymer exhibited a penetration threshold of roughly 83 J [1] which is only slightly higher compared to that of E151MWCNT1/GF. However, the improvement in MWCNT dispersion quality during the hand lay-up process could expectedly elevate this penetration threshold even further.

Overall, the addition of MWCNT significantly improved the low-velocity impact resistance of these laminate composites across the entire experimental testing's matrix, with the most dramatic improvements observed at high energy levels of 40 and 60 J. Thus, the simultaneous enhancement in peak load-bearing capacity, low absorbed energy, and high penetration threshold underscore the strong capability of MWCNTs to produce highly damage-tolerant Elium-based composite structures.

4.5 | Electrical Conductivity

The effect of MWCNT on the dielectric response of the laminate composites as a function of frequency is illustrated in Figure 9. Dielectric analysis is commonly used to characterize nonconductive materials, particularly polymers, according to frequency, temperature, and time, as reported in the literature [59]. The most fundamental dielectric characteristics are capacitance, electrical conductivity, and dielectric permittivity. Capacitance refers to the ability of a material to store electrical charges, while electrical conductivity reflects its capacity to permit the free movement of charge carriers. Dielectric permittivity

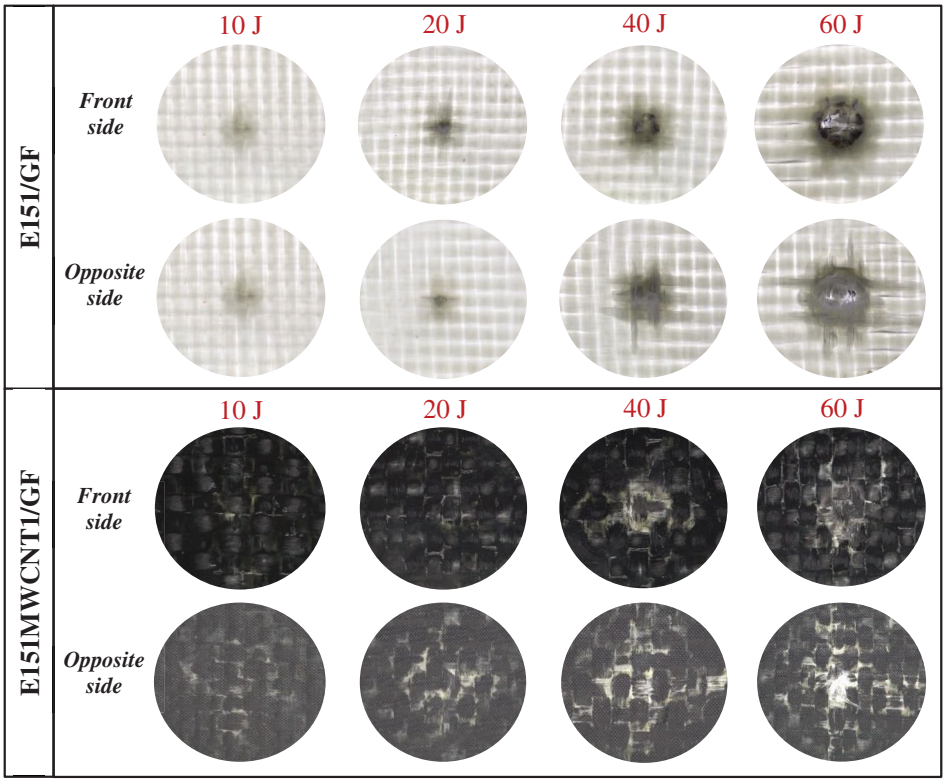

FIGURE 8 | Comparison of damage areas of 1 wt% MWCNT-reinforced composite with neat composite.

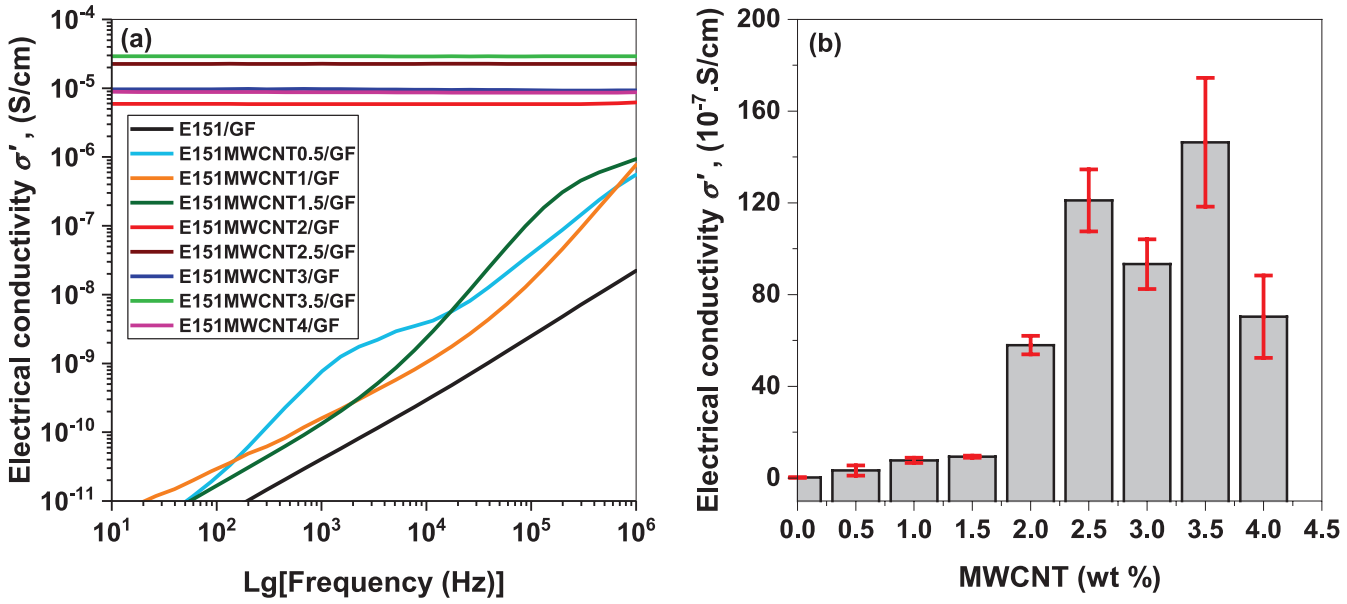

FIGURE 9 | Dielectric properties of laminated composites reinforced with MWCNT.

is defined as the response of a material to an external applied electric field, and it is closely linked to the polarizability of its microscopic constituents (atoms, molecules, polar groups, etc.). For dielectric polymers, the induced electric current essentially depends on both their electrical conductivity and dielectric permittivity. Studying the conductive properties of laminates composites containing MWCNT is essential because electrical measurements provide a real-time window into the internal microstructure, dispersion quality, and infiltration progress of the composite material. In this study, we focused on the electrical conductivity of laminate composites because it serves as the most sensitive metric for evaluating the uniformity of nanoparticle distribution throughout the laminate structure, particularly, when using hand lay-up processing. In addition, electrical conductivity highlights a specific interest of using MWCNT named percolation threshold. As reported in [17, 60], percolation involves effective random effective interconnections among uniformly distributed nanoparticles. At a certain fraction of linked particles, strong local transmission occurs which is defined as the percolation threshold.

As shown in Figure 9a, electrical conductivity follows two distinct trends. The first is an oblique linear trend around 10^2 Hz, clearly visible for E151/GF, indicating no electrical conductivity through this composite. With increasing MWCNT content from 0.5 to 1.5 wt%, the conductivity frequency decreased and the signal appeared in the form of curves, approximately linear and parallel to the neat composite trend. As results indicate, the initial increase in permittivity up to 1.5 wt% MWCNT, was insufficient to make the composite electrically conductive. The curve observed between 0 and 1.5 wt% MWCNT content demonstrate that the percolation threshold was not reached. In this concentration range, electric charges carriers cannot travel across the thickness of the laminate composite because MWCNT are not yet interconnected, as observed in Figure 1. Therefore, the deviations observed up to 2 wt% of MWCNT likely reflect a phase shift between conduction and polarization currents, which is probably caused by a poorer local dispersion of MWCNT.

Increase the MWCNT content in the composite further improve dielectric permittivity, leading to a much higher electrical conductivity at a concentration of 2 wt%. Due to the high interconnection probability of MWCNT, electrical charges can seamlessly move over long distances through the laminate material. Consequentially, the conductivity stabilizes, becoming flat and continuous, to form a distinct plateau. This confirms that the composites have officially transitioned into a conductive state. Beyond 2 wt% MWCNT, the laminate composites become increasingly conductive, as indicated by higher horizontal signals on the plot. This behavior suggests a high probability of interconnected MWCNT particles, shown in Figure 1e, where about 80% of the glass fabric surface was successfully impregnated. Thus, the electrical percolation threshold is definitely reached at 2 wt% MWCNT content. These observations are consistent with the quantitative electrical conductivity histogram shown in Figure 9b. Initially, electrical conductivity rose slightly from 0.21×10^{-7} to 9.3×10^{-7} S/cm, from E151/GF to E151MWCNT1.5/GF, respectively. This improvement of electrical conductivity was about 42.4%, compared to E151/GF. A sharp jump occurred at 2 wt% of MWCNT content, reaching a value of 58×10^{-7} S/cm which corresponds to an increase of 268.6%. Electrical conductivity further increased until it reached a maximum of 146.4×10^{-7} S/cm at 3.5 wt% of MWCNT content, despite minor dips at 3 and 4 wt% probably due to a less good uniform dispersion of MWCNT. The highest electrical conductivity obtained at 3.5 wt% of MWCNT content shows an exceptional enhancement of about 680%. Indeed, carbon nanotubes enhance the permittivity of polymer matrix composites and transform them into electrical conductors in several cases of use [18, 36, 60]. These results are consistent with the literature and they demonstrate a drastic enhancement of electrical conductivity due not only to the excellent conductive properties of MWCNT but also to the hand impregnation of glass fiber woven.

For all the composites studied, the properties mainly depended on MWCNT content and its dispersion on glass fibers. Direct comparison with literature is difficult, since glass fibers/Elium

acrylic laminates containing MWCNT have not yet been extensively studied. However, when compared to laminates based on thermosetting matrices [24, 27, 32, 36], the tensile properties (strength and Young's modulus) measured in this study are lower, but still significant. Moreover, the electrical conductivity obtained in this study at 2 wt% of MWCNT is about two times higher than that reported by Mendoue et al. [42].

Integrating MWCNT into Elium thermoplastic matrix successfully combines good mechanical strength (such as enhanced Young's modulus and impact resistance) with electrical conductivity and recyclability. In addition, these composite materials could also act as effective thermal conductors due to the high intrinsic thermal conductivity of MWCNT. Indeed, the nanotubes improve the thermal conductivity of the polymer matrix, which facilitates passive cooling for electronic components. Achieving all of these performances at once highlights the multifunctional nature of these MWCNT-reinforced laminate composites, making them highly suitable for lightweight structures that require smart and integrated functionalities. These MWCNT-reinforced materials offer strong potential for use in several advanced application areas. In aerospace engineering, they are suitable for primary and secondary structures, such as fuselages and wing leading edges, as well as electromagnetic interference (EMI) shielding to protect onboard electronic systems from radar or radio interference. For performance automotive applications, they are ideal for lightweight body and structural parts (such as bumper reinforcements, structural pillars, or engine cradles designed to lower fuel and energy consumption) and for thermal dissipation components. Finally, in clean energy industries, these materials are highly applicable for the manufacturing and structural reinforcement of hydrogen storage tanks.

It is important to note that the properties obtained in this study were highly dependent on the manufacturing process of the laminate composite. Therefore, the processing methods must be further refined to optimize the multifunctional performance of these MWCNT-containing composites, especially regarding the uniform dispersion of the nanotubes during the manual hand-impregnation step.

5 | Conclusion

This study investigates MWCNT-reinforced Elium acrylic laminate composites with various MWCNT contents ranging from 0.5 to 4 wt% to determine an optimal concentration that ensures both good mechanical and dielectric properties. The composite materials were manufactured using a vacuum resin infusion process after impregnating the bidirectional woven glass fibers that were manually preimpregnated with Graphistrength, using hand layup. The results showed that integrating MWCNT into the composite materials led to a slight decrease in the resin diffusion through woven glass fibers. This behavior resulted from particle agglomeration, which increased with higher MWCNT content. Microstructural analyses confirmed the presence of some aggregated particles within the laminate composites, likely due to the hand-impregnation process and the naturally pasty state of the raw MWCNTs. Despite localized aggregation, the addition of MWCNT proved highly beneficial for the tensile properties, due to the improvement of nominal stress, elongation at break, and Young's modulus. In the weft direction, at an optimal MWCNT content of 2.5 wt%, the nominal stress and Young's modulus improved on average by 4.57% and 13.31%, respectively, compared to the composite without MWCNT. In the warp direction, at an optimal MWCNT content of 2 wt%, the nominal stress and Young's modulus improved on average by 9% and 18% relative to the content. This improvement in elastic properties resulted from the high strength and Young's modulus of MWCNTs combined with good nanotube-to-fibers adhesion, which was aided by the manual hand-impregnating step. However, depending on the testing direction (warp versus weft), the elastic properties respectively decreased beyond 2 and 2.5 wt% of MWCNT content, probably due to stress concentrations caused by particle aggregates and weaker fibers–matrix adhesion. As for the low velocity impact response, the MWCNT-reinforced composites exhibited high peak forces, low absorbed energies, and high penetration thresholds. These improvements were particularly evident at higher impact energies of 40 and 60 J. At 40 J, the composite with 1.5 wt% MWCNT absorbed 16.40% less energy than the nonreinforced composite. At 60 J, the composite with 1.0 wt% MWCNT absorbed 10.24% less energy than the nonreinforced composite. Consequently, the 1.0 wt% MWCNT composite achieved a total penetration threshold of 76.65 J, representing an approximate 30% improvement over the composite without MWCNT.

The enhanced impact properties are attributed to strong fibers–matrix adhesion, driven by the tortuosity and the high toughness of MWCNTs. The nanotubes effectively created internal barriers that hindered crack propagation and absorbed deformation energy. The MWCNT-reinforced composites transitioned into electrical conductors starting exactly at 2 wt% MWCNT, where they exhibited a 269% increase in electrical conductivity compared to the composite without MWCNT, marking the system's electrical percolation threshold. An exceptionally improvement of 680% in electrical conductivity was achieved at higher concentration of 3.5 wt% of MWCNT, highlighting the remarkable ability of these nanotubes to render the Elium composites highly conductive. Ultimately, using MWCNT at moderate concentrations (between 0.5 and 2.5 wt%) successfully enhances the mechanical and dielectric properties of Elium acrylic laminate composites. Based on the comprehensive data gathered in this study, adding 2 wt% of MWCNT could represent the ideal, optimal concentration for impregnating well-balanced, multifunctional composite structures.

Author Contributions

A. Y. E. Kouassi: investigation, writing – original draft, validation, writing – review and editing, software, formal analysis, data curation. **R. Matadi Boumbimba:** funding acquisition, project administration, writing – review and editing, supervision, validation. **M. K. Sangaré:** methodology, formal analysis, investigation, writing – review and editing. **I. Royaud:** funding acquisition, supervision, writing – review and editing. **T. Libura:** funding acquisition, supervision, writing – review and editing. **P. Dziewit:** supervision, writing – review and editing. **M. Wary:** investigation, writing – review and editing, funding acquisition.

Acknowledgments

We thank Pierre GERARD, Mathieu BHEIR, and Audrey LE-FICHANT for their help to processing laminate composites.

Conflicts of Interest

The authors declare no conflicts of interest.

Data Availability Statement

Additional data on vacuum resin infusion, resin diffusion, and tensile damage patterns are available in Supporting Information. Another data set will be made available upon written request to the corresponding author.

References

1. G. Kinvi-Dossou, R. Matadi Boumbimba, N. Bonfoh, et al., "Innovative Acrylic Thermoplastic Composites Versus Conventional Composites: Improving the Impact Performances," *Composite Structures* 217 (2019): 1–13, https://doi.org/10.1016/j.compstruct.2019.02.090.

2. Z. Boufaida, L. Farge, S. André, and Y. Meshaka, "Influence of the Fiber/Matrix Strength on the Mechanical Properties of a Glass Fiber/Thermoplastic-Matrix Plain Weave Fabric Composite," *Composites Part A: Applied Science and Manufacturing* 75 (2015): 28–38, https://doi.org/10.1016/j.compositesa.2015.04.012.

3. G. Kinvi-Dossou, R. Matadi Boumbimba, N. Bonfoh, Y. Koutsawa, D. Eccli, and P. Gerard, "A Numerical Homogenization of E-Glass/Acrylic Woven Composite Laminates: Application to Low Velocity Impact," *Composite Structures* 200 (2018): 540–554, https://doi.org/10.1016/j.compstruct.2018.05.137.

4. G. Kinvi-Dossou, N. Bonfoh, R. Matadi Boumbimba, et al., "A Mesoscale Modelling Approach of Glass Fibre/Elium Acrylic Woven Laminates for Low Velocity Impact Simulation," *Composite Structures* 252 (2020): 112671, https://doi.org/10.1016/j.compstruct.2020.112671.

5. N. Koumba, R. M. Boumbimba, N. Bonfoh, F. Eba, and M. Wary, "Effect of Reparation on the Mechanical Behavior of Glass Fibers/E Lium Acrylic Laminate Composites: Experimental and Numerical Approaches," *Polymer Composites* 45, no. 7 (2024): 6385–6403, https://doi.org/10.1002/pc.28204.

6. R. Matadi Boumbimba, C. Froustey, P. Viot, and P. Gerard, "Low Velocity Impact Response and Damage of Laminate Composite Glass Fibre/Epoxy Based Tri-Block Copolymer," *Composites. Part B, Engineering* 76 (2015): 332–342, https://doi.org/10.1016/j.compositesb.2015.02.007.

7. M. Bashar, U. Sundararaj, and P. Mertiny, "Study of Matrix Micro-Cracking in Nano Clay and Acrylic Tri-Block-Copolymer Modified Epoxy/Basalt Fiber-Reinforced Pressure-Retaining Structures," *Express Polymer Letters* 5, no. 10 (2011): 882–896, https://doi.org/10.3144/expresspolymlett.2011.87.

8. T. Gómez-del Río, A. Salazar, R. A. Pearson, and J. Rodríguez, "Fracture Behaviour of Epoxy Nanocomposites Modified With Triblock Copolymers and Carbon Nanotubes," *Composites. Part B, Engineering* 87 (2016): 343–349, https://doi.org/10.1016/j.compositesb.2015.08.085.

9. R. Matadi Boumbimba, M. Coulibaly, A. Khabouchi, G. Kinvi-Dossou, N. Bonfoh, and P. Gerard, "Glass Fibres Reinforced Acrylic Thermoplastic Resin-Based Tri-Block Copolymers Composites: Low Velocity Impact Response at Various Temperatures," *Composite Structures* 160 (2017): 939–951, https://doi.org/10.1016/j.compstruct.2016.10.127.

10. A. Y. E. Kouassi, M. K. Sangaré, R. Matadi Boumbimba, N. Koumba, and P. Gerard, "Experimental and Multiscale Investigation of the Elastic and Impact Properties of Glass Fibers/Elium Acrylic Modified Nanoparticles Laminate Composites," *Materials Letters* 354 (2024): 135369, https://doi.org/10.1016/j.matlet.2023.135369.

11. A. Y. E. Kouassi, R. Matadi Boumbimba, and M. K. Sangaré, "Effect of the Nanostrength M53 on Elastic Properties of Glass Fiber Reinforced Acrylic Thermoplastic Resin," in *Advances in Applied Mechanics. Lecture Notes in Mechanical Engineering*, ed. Z. Azari, K. El Had, M. E. Ait Ali, A. El Mahi, F. Chaari, and M. Haddar (Springer Nature Switzerland, 2024), 1–15, https://doi.org/10.1007/978-3-031-49727-8_1.

12. M. Samet, A. Kallel, and A. Serghei, "Polymer Bilayers With Enhanced Dielectric Permittivity and Low Dielectric Losses by Maxwell–Wagner–Sillars Interfacial Polarization: Characteristic Frequencies and Scaling Laws," *Journal of Applied Polymer Science* 136, no. 22 (2019): 47551, https://doi.org/10.1002/app.47551.

13. S. Rathinavel, K. Priyadharshini, and D. Panda, "A Review on Carbon Nanotube: An Overview of Synthesis, Properties, Functionalization, Characterization, and the Application," *Materials Science and Engineering B* 268 (2021): 115095, https://doi.org/10.1016/j.mseb.2021.115095.

14. B. Shivamurthy, S. Anandhan, K. U. Bhat, and B. H. S. Thimmappa, "Structure-Property Relationship of Glass Fabric/MWCNT/Epoxy Multi-Layered Laminates," *Composites Communications* 22 (2020): 100460, https://doi.org/10.1016/j.coco.2020.100460.

15. M. MD Nadeem, S. Chethan, K. Srinivasa, M. Karthik Kumar, and N. Yathisha, "Effect of Glass Fibers and Multi Walled Carbon Nano Tubes (MWCNT'S) on Mechanical Properties of Epoxy Hybrid Composites at Elevated Temperature," *Materials Today: Proceedings* 44 (2021): 2013–2018, https://doi.org/10.1016/j.matpr.2020.12.123.

16. A. M. Díez-Pascual, M. Naffakh, C. Marco, M. A. Gómez-Fatou, and G. J. Ellis, "Multiscale Fiber-Reinforced Thermoplastic Composites Incorporating Carbon Nanotubes: A Review," *Current Opinion in Solid State & Materials Science* 18, no. 2 (2014): 62–80, https://doi.org/10.1016/j.cossms.2013.06.003.

17. S. Tamayo-Vegas, A. Muhsan, M. Tarfaoui, K. Lafdi, and L. Chang, "Effect of CNT Additives on the Electrical Properties of Derived Nanocomposites (Experimentally and Numerical Investigation)," *Materials Today Proceedings* 52 (2021): 199–205, https://doi.org/10.1016/j.matpr.2021.09.361.

18. I. Bouknaitir, N. Aribou, S. A. Elhad Kassim, et al., "Electrical Properties of Conducting Polymer Composites: Experimental and Modeling Approaches," *Spectroscopy Letters* 50, no. 4 (2017): 196–199, https://doi.org/10.1080/00387010.2017.1282522.

19. M. A. Maghsoudlou, R. Barbaz Isfahani, S. Saber-Samandari, and M. Sadighi, "Effect of Interphase, Curvature and Agglomeration of SWCNTs on Mechanical Properties of Polymer-Based Nanocomposites: Experimental and Numerical Investigations," *Composites. Part B, Engineering* 175 (2019): 107119, https://doi.org/10.1016/j.compositesb.2019.107119.

20. A. B. Dalton, S. Collins, E. Muñoz, et al., "Super-Tough Carbon-Nanotube Fibres," *Nature* 423, no. 6941 (2003): 703, https://doi.org/10.1038/423703a.

21. P. Miaudet, S. Badaire, M. Maugey, et al., "Hot-Drawing of Single and Multiwall Carbon Nanotube Fibers for High Toughness and Alignment," *Nano Letters* 5, no. 11 (2005): 2212–2215, https://doi.org/10.1021/nl051419w.

22. A. O. Fulmali, R. N. Kar, B. C. Ray, and R. K. Prusty, "Superior Flexural, Interlaminar- Shear and Fracture Performance of Glass Fiber/Epoxy Laminates Employing 3-D Reinforcement Approach: Emphasis on Through Thickness Functionalized CNT Alignment," *Composites Part A: Applied Science and Manufacturing* 175 (2023): 107795, https://doi.org/10.1016/j.compositesa.2023.107795.

23. R. K. Prusty, D. K. Rathore, and B. C. Ray, "Evaluation of the Role of Functionalized CNT in Glass Fiber/Epoxy Composite at Above- and Sub-Zero Temperatures: Emphasizing Interfacial Microstructures," *Composites Part A: Applied Science and Manufacturing* 101 (2017): 215–226, https://doi.org/10.1016/j.compositesa.2017.06.020.

24. M. Dheepthi, P. M. Radhakrishnan, and R. Santhanakrishnan, "Effect of MWCNTs on Mechanical Properties of Woven Cross Ply GFRP Laminates," *Materials Today Proceedings* (2023): S2214785323005126, https://doi.org/10.1016/j.matpr.2023.01.416.

25. W. A. D. W. Dalina, S. H. Tan, and M. Mariatti, "Properties of Fiberglass/MWCNT Buckypaper/Epoxy Laminated Composites," *Procedia*

Chemistry 19 (2016): 935–942, https://doi.org/10.1016/j.proche.2016.03.138.

26. J. Karger-Kocsis, H. Mahmood, and A. Pegoretti, "Recent Advances in Fiber/Matrix Interphase Engineering for Polymer Composites," *Progress in Materials Science* 73 (2015): 1–43, https://doi.org/10.1016/j.pmatsci.2015.02.003.

27. K. Yoganandam, K. Premkumar, V. Alagumalai, J. Lin, V. Shanmugam, and O. Das, "Quasi-Static Puncture Shear Loading Behaviour MWCNT/Glass Fibre Epoxy Laminates With Various Indenters," *Polymer Testing* 127 (2023): 108191, https://doi.org/10.1016/j.polymertesting.2023.108191.

28. A. Gaurav and K. K. Singh, "Ilss Improvement of Quasi-Isotropic Glass Fiber Reinforced Epoxy Laminate Enhanced With Arc Discharged Multi-Walled Carbon Nanotubes," *Materials Today Proceedings* 5, no. 2 (2018): 8638–8644, https://doi.org/10.1016/j.matpr.2017.11.563.

29. N. Domun, H. Hadavinia, T. Zhang, T. Sainsbury, G. H. Liaghat, and S. Vahid, "Improving the Fracture Toughness and the Strength of Epoxy Using Nanomaterials – A Review of the Current Status," *Nanoscale* 7, no. 23 (2015): 10294–10329, https://doi.org/10.1039/C5NR01354B.

30. C. S. Grimmer and C. K. H. Dharan, "High-Cycle Fatigue of Hybrid Carbon Nanotube/Glass Fiber/Polymer Composites," *Journal of Materials Science* 43, no. 13 (2008): 4487–4492, https://doi.org/10.1007/s10853-008-2651-9.

31. M. R. Loos and I. Manas-Zloczower, "Reinforcement Efficiency of Carbon Nanotubes – Myth and Reality," *Macromolecular Theory and Simulations* 21, no. 2 (2012): 130–137, https://doi.org/10.1002/mats.201100099.

32. P. M. Radhakrishnan and K. Ramajeyathilagam, "Effect of MWCNTs on Mechanical Properties of Woven Angle Ply GFRP Laminates," *Materials Today Proceedings* (2023): S2214785323045820, https://doi.org/10.1016/j.matpr.2023.08.301.

33. K. K. Singh, M. T. A. Ansari, and M. S. Azam, "Fatigue Life and Damage Evolution in Woven GFRP Angle Ply Laminates," *International Journal of Fatigue* 142 (2021): 105964, https://doi.org/10.1016/j.ijfatigue.2020.105964.

34. Y. He, S. Yang, H. Liu, et al., "Reinforced Carbon Fiber Laminates With Oriented Carbon Nanotube Epoxy Nanocomposites: Magnetic Field Assisted Alignment and Cryogenic Temperature Mechanical Properties," *Journal of Colloid and Interface Science* 517 (2018): 40–51, https://doi.org/10.1016/j.jcis.2018.01.087.

35. N. H. Ismail, J. O. Akindoyo, and M. Mariatti, "Solvent Mediated Dispersion of Carbon Nanotubes for Glass Fibre Surface Modification—Suspensions Stability and Its Effects on Mechanical, Interlaminar and Dynamic Mechanical Properties of Modified Glass Fibre Reinforced Epoxy Laminates," *Composites Part A: Applied Science and Manufacturing* 139 (2020): 106091, https://doi.org/10.1016/j.compositesa.2020.106091.

36. E. J. Jelmy, M. Lakshmanan, and N. K. Kothurkar, "Microwave Absorbing Behavior of Glass Fiber Reinforced MWCNT-PANi/Epoxy Composite Laminates," *Materials Today Proceedings* 26 (2020): 36–43, https://doi.org/10.1016/j.matpr.2019.04.203.

37. M. M. Rahman, S. Zainuddin, M. V. Hosur, et al., "Improvements in Mechanical and Thermo-Mechanical Properties of e-Glass/Epoxy Composites Using Amino Functionalized MWCNTs," *Composite Structures* 94, no. 8 (2012): 2397–2406, https://doi.org/10.1016/j.compstruct.2012.03.014.

38. J. Xu, P. Yao, Z. Jiang, et al., "Preparation, Morphology, and Properties of Conducting Polyaniline-Grafted Multiwalled Carbon Nanotubes/Epoxy Composites," *Journal of Applied Polymer Science* 125, no. S1 (2012): E334–E341, https://doi.org/10.1002/app.35677.

39. D. He, D. Salem, J. Cinquin, G. P. Piau, and J. Bai, "Impact of the Spatial Distribution of High Content of Carbon Nanotubes on the Electrical Conductivity of Glass Fiber Fabrics/Epoxy Composites Fabricated by RTM Technique," *Composites Science and Technology* 147 (2017): 107–115, https://doi.org/10.1016/j.compscitech.2017.05.012.

40. K. Mohan and T. Rajmohan, "Effects of MWCNT on Mechanical Properties of Glass-Flax Fiber Reinforced Nano Composites," *Materials Today Proceedings* 5, no. 5 (2018): 11628–11635, https://doi.org/10.1016/j.matpr.2018.02.133.

41. M. Kim, T. W. Lee, S. M. Park, and Y. G. Jeong, "Structures, Electrical and Mechanical Properties of Epoxy Composites Reinforced With MWCNT-Coated Basalt Fibers," *Composites Part A: Applied Science and Manufacturing* 123 (2019): 123–131, https://doi.org/10.1016/j.compositesa.2019.05.011.

42. D. K. Mendoue, A. Benelfellah, R. M. Boumbimba, et al., "Study of the Thermomechanical Behavior of Composite Based on ELIUM Acrylic Resin, Carbon Nanotubes, and Flax Fibers: Experimental Approach," *Polymer Composites* 45, no. 13 (2024): 11785–11803, https://doi.org/10.1002/pc.28597.

43. W. Obande, C. M. Ó. Brádaigh, and D. Ray, "Continuous Fibre-Reinforced Thermoplastic Acrylic-Matrix Composites Prepared by Liquid Resin Infusion—A Review," *Composites. Part B, Engineering* 215 (2021): 108771, https://doi.org/10.1016/j.compositesb.2021.108771.

44. T. Libura, R. Matadi Boumbimba, A. Rusinek, Z. L. Kowalewski, T. Szymczak, and P. Gerard, "Effect of Uniaxial Fatigue Aging and Fabric Orientation on Low Impact Velocity Response of Glass Fibers/Elium Acrylic Composite Laminates," *Materials* 14, no. 15 (2021): 4089, https://doi.org/10.3390/ma14154089.

45. N. Coppey, L. Noé, M. Monthioux, and B. Caussat, "Decorated Carbon Nanotubes by Silicon Deposition in Fluidized Bed for Li-Ion Battery Anodes," *Chemical Engineering Research and Design* 91, no. 12 (2013): 2491–2496, https://doi.org/10.1016/j.cherd.2013.01.002.

46. Y. Piao, V. N. Tondare, C. S. Davis, et al., "Comparative Study of Multiwall Carbon Nanotube Nanocomposites by Raman, SEM, and XPS Measurement Techniques," *Composites Science and Technology* 208 (2021): 108753, https://doi.org/10.1016/j.compscitech.2021.108753.

47. D. Leonavičius, I. Pundienė, G. Girskas, J. Pranckevičienė, M. Kligys, and A. Kairytė, "The Effect of Multi-Walled Carbon Nanotubes on the Rheological Properties and Hydration Process of Cement Pastes," *Construction and Building Materials* 189 (2018): 947–954, https://doi.org/10.1016/j.conbuildmat.2018.09.082.

48. P. Verge, S. Benali, L. Bonnaud, et al., "Unpredictable Dispersion States of MWNTs in HDPE: A Comparative and Comprehensive Study," *European Polymer Journal* 48, no. 4 (2012): 677–683, https://doi.org/10.1016/j.eurpolymj.2012.01.002.

49. A. Forcellese, M. Simoncini, A. Vita, A. Giovannelli, and L. Leonardi, "Performance Analysis of MWCNT/Epoxy Composites Produced by CRTM," *Journal of Materials Processing Technology* 286 (2020): 116839, https://doi.org/10.1016/j.jmatprotec.2020.116839.

50. L. Meszaros, I. M. Gali, T. Czigany, and T. Czvikovszky, "Effect of Nanotube Content on Mechanical Properties of Basalt Fibre Reinforced Polyamide 6," *Plastics, Rubber and Composites* 40, no. 6–7 (2011): 289–293, https://doi.org/10.1179/1743289810Y.0000000015.

51. A. Gaurav and K. K. Singh, "Effect of Pristine MWCNTs on the Fatigue Life of GFRP Laminates-An Experimental and Statistical Evaluation," *Composites. Part B, Engineering* 172 (2019): 83–96, https://doi.org/10.1016/j.compositesb.2019.05.069.

52. K. B. N. V. S. Ganesh Gupta, A. Yadav, M. M. Hiremath, R. K. Prusty, and B. C. Ray, "Enhancement of Mechanical Properties of Glass Fiber Reinforced Vinyl Ester Composites by Embedding Multi-Walled Carbon Nanotubes Through Solution Processing Technique," *Materials Today Proceedings* 27 (2020): 1045–1050, https://doi.org/10.1016/j.matpr.2020.01.391.

53. B. Sen, A. O. Fulmali, K. B. N. V. S. G. Gupta, R. K. Prusty, and B. C. Ray, "A Study of the Effect of Carbon Nanotube/Nanoclay Binary Nanoparticle Reinforcement on Glass Fibre/Epoxy Composites,"

Materials Today Proceedings 26 (2020): 2026–2031, https://doi.org/10.1016/j.matpr.2020.02.440.

54. W. Han, J. Zhou, and Q. Shi, "Research Progress on Enhancement Mechanism and Mechanical Properties of FRP Composites Reinforced With Graphene and Carbon Nanotubes," *Alexandria Engineering Journal* 64 (2023): 541–579, https://doi.org/10.1016/j.aej.2022.09.019.

55. C. M. Meenakshi and A. Krishnamoorthy, "Preparation and Mechanical Characterization of Flax and Glass Fiber Reinforced Polyester Hybrid Composite Laminate by Hand Lay-Up Method," *Materials Today Proceedings* 5, no. 13 (2018): 26934–26940, https://doi.org/10.1016/j.matpr.2018.08.181.

56. N. M. Nurazzi, F. A. Sabaruddin, M. M. Harussani, et al., "Mechanical Performance and Applications of CNTs Reinforced Polymer Composites—A Review," *Nanomaterials* 11, no. 9 (2021): 2186, https://doi.org/10.3390/nano11092186.

57. L. Aktas, Y. K. Hamidi, and M. C. Altan, "Dispersion Characterization of Nanoclay in Molded Epoxy Disks by Combined Image Analysis and Wavelength Dispersive Spectrometry," *Journal of Engineering Materials and Technology* 130, no. 3 (2008): 031005, https://doi.org/10.1115/1.2931140.

58. P. N. B. Reis, J. A. M. Ferreira, Z. Y. Zhang, T. Benameur, and M. O. W. Richardson, "Impact Response of Kevlar Composites With Nanoclay Enhanced Epoxy Matrix," *Composites. Part B, Engineering* 46 (2013): 7–14, https://doi.org/10.1016/j.compositesb.2012.10.028.

59. F. Kremer and A. Schönhals, *Broadband Dielectric Spectroscopy* (Springer Berlin Heidelberg, 2003), https://doi.org/10.1007/978-3-642-56120-7.

60. S. Demski, K. Dydek, K. Bartnicka, K. Majchrowicz, R. Kozera, and A. Boczkowska, "Introduction of SWCNTs as a Method of Improvement of Electrical and Mechanical Properties of CFRPs Based on Thermoplastic Acrylic Resin," *Polymers* 15, no. 3 (2023): 506, https://doi.org/10.3390/polym15030506.

Supporting Information

Additional supporting information can be found online in the Supporting Information section. **Figure SI:-1.** Vacuum resin infusion process for MWCNT-based laminate composites. **Figure SI:-2** Illustration of resin diffusion in glass fabrics. **Figure SI:-3** Tensile specimen damage patterns at 1 mm/min loading rate.